Rainfall Sensitivity to Microphysics and Planetary Boundary Layer Parameterizations in Convection-Permitting Simulations over Northwestern South America

K. Santiago HERNÁNDEZ[1*], Sebastián GÓMEZ-RÍOS[1], Juan J. HENAO[1,3], Vanessa ROBLEDO[1], Álvaro RAMÍREZ-CARDONA[1], and Angela M. RENDÓN[1,2]

1 *Geolimna*, *Escuela Ambiental*, *Facultad de Ingeniería*, *Universidad de Antioquia*, *Medellín* 050010, *Colombia*
2 *Grupo de Ingeniería y Gestión Ambiental (GIGA)*, *Escuela Ambiental*, *Facultad de Ingeniería*, *Universidad de Antioquia*, *Medellín* 050010, *Colombia*
3 *Division of Atmospheric Sciences*, *Desert Research Institute*, *Reno*, *NV* 89512, *USA*

(Received 5 September 2023; in final form 15 March 2024)

ABSTRACT

Convection-permitting modeling allows us to understand mechanisms that influence rainfall in specific regions. However, microphysics parameterization (MP) and planetary boundary layer (PBL) schemes remain an important source of uncertainty, affecting rainfall intensity, occurrence, duration, and propagation. Here, we study the sensitivity of rainfall to three MP [Weather Research and Forecasting (WRF) Single-Moment 6-class (WSM6), Thompson, and Morrison] and two PBL [the Yonsei University (YSU) and Mellor–Yamada Nakanishi Niino (MYNN)] schemes with a convection-permitting resolution (4 km) over northwestern South America (NWSA). Simulations were performed by using the WRF model and the results were evaluated against soundings, rain gauges, and satellite data, considering the spatio-temporal variability of rainfall over diverse regions prone to deep convection in NWSA. MP and PBL schemes largely influenced simulated rainfall, with better results for the less computationally expensive WSM6 MP and YSU PBL schemes. Regarding rain gauges and satellite estimates, simulations with Morrison MP overestimated rainfall, especially westward of the Andes, whereas the MYNN PBL underestimated precipitation in the Amazon–Savannas flatlands. We found that the uncertainty in the rainfall representation is highly dependent on the region, with a higher influence of MP in the Colombian Pacific and PBL in the Amazon–Savannas flatlands. When analyzing rainfall-related processes, the selection of both MP and PBL parameterizations exerted a large influence on the simulated lower tropospheric moisture flux and moisture convergence. PBL schemes significantly influenced the downward shortwave radiation, with MYNN simulating a greater amount of low clouds, which decreased the radiation income. Furthermore, latent heat fluxes were greater for YSU, favoring moist convection and rainfall. MP schemes had a marked impact on vertical velocity. Specifically, Morrison MP showed stronger convection and higher precipitation rates, which is associated with a greater latent heat release due to solid-phase hydrometeor formation. This study provides insights into assessing physical parameterizations in numerical models and suggests key processes for rainfall representation in NWSA.

Key words: sensitivity, microphysics, planetary boundary layer (PBL), Weather Research and Forecasting (WRF), processes

Citation: Hernández, K. S., S. Gómez-Ríos, J. J. Henao, et al., 2024: Rainfall sensitivity to microphysics and planetary boundary layer parameterizations in convection-permitting simulations over northwestern South America. *J. Meteor. Res.*, **38**(4), 805–825, doi: 10.1007/s13351-024-3156-4.

1. Introduction

Precipitation is essential for water security and risk management. Numerical models are helpful tools for understanding non-linear and highly complex processes, mechanisms, and environments associated with rainfall occurrence at various scales. However, some processes that occur at a sub-grid scale (higher resolutions than those of models), such as microphysics, boundary layer fluxes, and cumulus formation, need to be parameterized,

Supported by the Patrimonio Autónomo Fondo Nacional de Financiamiento para la Ciencia, la Tecnología y la Innovación, Fondo Francisco José de Caldas from the Colombian Ministry of Science, Technology, and Innovation (MINCIENCIAS, 1115-852-70955). Open Access funding provided by Colombia Consortium.

*Corresponding author: ksantiago.hernandez@udea.edu.co

which add uncertainty to model results (Stensrud, 2007). Specifically for precipitation, simulations with cumulus parameterizations turned off (convection-permitting simulations) usually give better results than simulations using convection parameterizations (Woodhams et al., 2018; Gutowski et al., 2020). In addition to cumulus convection schemes, the impact of microphysics and boundary layer processes has also been highlighted in rainfall representation (Karki et al., 2018; Srinivas et al., 2018).

Microphysics parameterizations (MP) account for small-scale processes that determine the formation and growth of hydrometeor species, which govern the cloud particle populations and are highly relevant for precipitation development (Morrison et al., 2020). Furthermore, the phase changes of water vapor, also represented by MP schemes, affect the latent and sensible heat fluxes (Morrison et al., 2020), influence the atmospheric dynamics (Efstathiou et al., 2013), and induce convective patterns. There are different approaches to parameterize cloud microphysics, including "bulk" schemes that simulate the mixing ratio (single moment) or both the mixing ratio and number concentration (double moment) for different hydrometeor species, and "spectral" (or bin) schemes that represent the hydrometeor population including the particle size distribution (Khain et al., 2015; Morrison et al., 2020). As bin schemes have a more detailed representation of microphysical processes, they are computationally more expensive, making them less viable for operational tasks and even research.

Several studies have shown high sensitivity of rainfall representation to MP schemes (Feng et al., 2018; Martínez-Castro et al., 2019; Das et al., 2021). In fact, MP are crucial to adequately forecast the characteristics of severe storms (Gorja et al., 2023; Shu et al., 2023) and tropical cyclones (Mohan et al., 2019; Zhao et al., 2020). Simulating an extreme rainfall event on the Korean Peninsula with four MP schemes, Jo et al. (2023) found large differences in accumulated rainfall and the time and location of maximum rainfall. Similarly, Liu et al. (2018) found that MP modifies rainfall amounts, stratiform rainfall production, and cloud properties. For a severe rainfall event in India, Thomas et al. (2021) exhibited high sensitivity to MP schemes, impacting thermodynamic profiles and convection. Feng et al. (2018) studied representation of mesoscale convective systems (MCSs) by different MP schemes, demonstrating the role of diabatic heating in enhancing mid-level convergence that contributes to form more long-lived MCSs. Furthermore, Huang et al. (2020) studied how different bulk MP schemes impact the simulation of an extreme rainfall event in China. Sensitivities were also associated with differences in the latent heat released and the evaporative cooling.

On the other hand, planetary boundary layer (PBL) processes determine the exchange of momentum, energy, and moisture between the earth's surface and the free atmosphere, which plays a crucial role in rainfall development. PBL processes are turbulent and highly non-linear owing to the heterogeneity of the terrain and the surface differential heating (Lehner and Rotach, 2018). There are two main approaches to parameterize turbulent fluxes in the boundary layer, namely local and non-local closure schemes (Cohen et al., 2015). Local PBL schemes use conditions and gradients in each vertical layer to estimate fluxes (Nakanishi and Niino, 2006), assuming that turbulence is analogous to molecular diffusion, while non-local schemes consider conditions throughout the boundary layer (Hong et al., 2006b), acknowledging that turbulence is a superposition of eddies of different scales, such that larger eddies can transport fluid across a finite distance before smaller eddies can cause mixing (Stull, 1988). Previous studies have assessed the impact of PBL schemes using these two approaches (Que et al., 2016; Comin et al., 2021; Zhu et al., 2022), with non-local schemes producing larger vertical mixing and rainfall.

Notable sensitivities among PBL schemes in determining the rainfall's timing, intensity, and spatial distribution have been previously reported (Klein et al., 2015; Qian et al., 2016; Chawla et al., 2018; Srinivas et al., 2018). Taraphdar and Pauluis (2021) even found a higher sensitivity to PBL than to MP schemes in the rainfall simulation, with differences of up to 40% in total rainfall when using different PBL schemes. In tropical regions, the selection of PBL schemes significantly impacts simulated moisture fluxes, convective initiation, and precipitation (Qian et al., 2016). Also, simulating an extreme rainfall event in India, Srinivas et al. (2018) showed that the PBL schemes changed the upper atmosphere circulation, energy transport, moisture convergence, and convection intensity. Recently, Hu et al. (2023) studied the relationship between vertical mixing clouds and precipitation in the Amazon basin, finding that PBL schemes impact daytime cloud dissipation, influencing downward radiation, convective available potential energy (CAPE), and rainfall. Evaluating the representation of MCSs, Prein et al. (2022) reported a high dependence on MP in the Great Plains, but more sensitivity to PBL in the Amazon basin, which reflects the importance of evaluating the performance of distinct groups of schemes in different regions.

In northwestern South America (NWSA), a region of intense convection and high rainfall occurrence (Jaramillo et al., 2017; Hernández-Deckers, 2022), previous studies have shown the impacts of MP and PBL paramet-

erization schemes on rainfall representation. Moya-Álvarez et al. (2020) studied the influence of PBL schemes on rainfall forecasting in the central Andes of Perú and found significant differences in convection between schemes, conditioning rainfall amounts. In the Ecuadorian Andes, Junquas et al. (2022) highlighted a marked influence on the diurnal behavior of rain of different MPs. In Colombia, it has been reported that the selection of MP schemes affected rainfall propagation offshore of the Colombian Pacific coast (Yepes et al., 2020). Also, while studying the moisture transport by the Orinoco low-level jet (LLJ), Martínez et al. (2022) found that the selection of PBL parameterization induced differences not only in horizontal moisture flux but also in downwind precipitation. In the same way, for a sensitivity analysis between three MP schemes, Gomez-Rios et al. (2023) showed spatiotemporal differences in rainfall patterns in the inter-Andean Magdalena valley.

More specifically, some extreme precipitation events related to strong convection have been reported in Colombia with important implications on infrastructure and human lives loss, such as those in Salgar in 2015 (Hoyos et al., 2019) and Mocoa in 2017 (Martínez et al., 2021). Moreover, although previous sensitivity studies exist for the region, they do not analyze the processes behind the representation of precipitation, are developed for specific regions, or do not perform convection-permitting simulations, which show the need to strengthen the modeling experiments for understanding physics controlling rainfall in Colombia and NWSA.

In this work, we study the sensitivity of rainfall to MP and PBL schemes in NWSA at convection-permitting resolution (4 km), involving an analysis of key processes behind rainfall, such as cloud cover fraction and vertical distribution, moisture transport, and latent heat release. Simulations are performed with the Weather Research and Forecasting (WRF) model and evaluated against satellite data, which are helpful both for model evaluation and elucidating regions with higher sensitivity. The remainder of the document is structured as follows. Section 2 presents the description of the study area and the modeling experiment. Section 3 contains the evaluation of the model parameterizations, the analysis of processes that control the sensitivity, and discusses the main results in the light of previous studies. Finally, Section 4 is the conclusions of this study.

2. Data and methods

2.1 *Study area and period*

NWSA is a tropical region in the northernmost part of South America (Fig. 1) with a hydroclimatology driven mainly by the meridional shift of the Intertropical Convergence Zone (ITCZ) and by the seasonal variations of three LLJs known as the Caribbean, Orinoco, and Choco jets (Poveda et al., 2006; Torrealba Rincón and Amador Astúa, 2010; Poveda et al., 2014; Builes-Jaramillo et al., 2022). The Andes mountain range crosses the region into three branches, forming environments that favor convection and rainfall (Rydbeck et al., 2017; Gomez-Rios et al., 2023). The combination of these factors causes high spatiotemporal variability of convection and precipitation in NWSA.

According to previous studies, some regions in NWSA are prone to deep convection and rainfall occurrence (Jaramillo et al., 2017; Urrea et al., 2019; Hernández-Deckers, 2022): (1) the Colombian Pacific coast (Yepes et al., 2019; Mejía et al., 2021), which is known as one of the rainiest places on earth and where the Choco LLJ takes place; (2) the Magdalena valley (Hernández-Deckers, 2022; Gomez-Rios et al., 2023), with strong localized convection due to intra-valley processes; (3) the Colombian Caribbean coast (Albrecht et al., 2016; Martínez et al., 2021), a lightning hotspot where sea–land breezes interact with topography causing moist convection; (4) the gulf of Maracaibo in Venezuela (Albrecht et al., 2016; Hernández-Deckers, 2022), another well-known lightning hotspot; and (5) the Amazon-Orinoco basins (Builes-Jaramillo et al., 2022; Martínez et al., 2022), two vast and relatively flat regions with LLJ influence and high precipitation rates. Figure 1 shows these six regions in which we focused our assessment.

The model simulations were performed during a 7-day period (18–25 September 2019). The simulation period was relatively short due to the computational burden of convection-permitting simulations; however, this period was carefully selected to perform the sensitivity analysis for two main reasons: i) the relatively short but information intensive OTREC (Organization of Tropical East Pacific Convection) field campaign (Fuchs-Stone et al., 2020) included this period, with available data from soundings at two regions with high convective activity, but scarce observations, which are Nuquí in the Pacific coast and Puerto Triunfo in the Magdalena valley (Fig. 1); and ii) the high and widespread convective activity in September for NWSA (Hernández-Deckers, 2022), especially during the study period, which exhibited significant convective events across the regions (Supplementary in Fig. S1).

2.2 *Modeling experiment*

The WRF model v4.2 (Skamarock et al., 2019) was used in this study, following a two-domain (one-way nes-

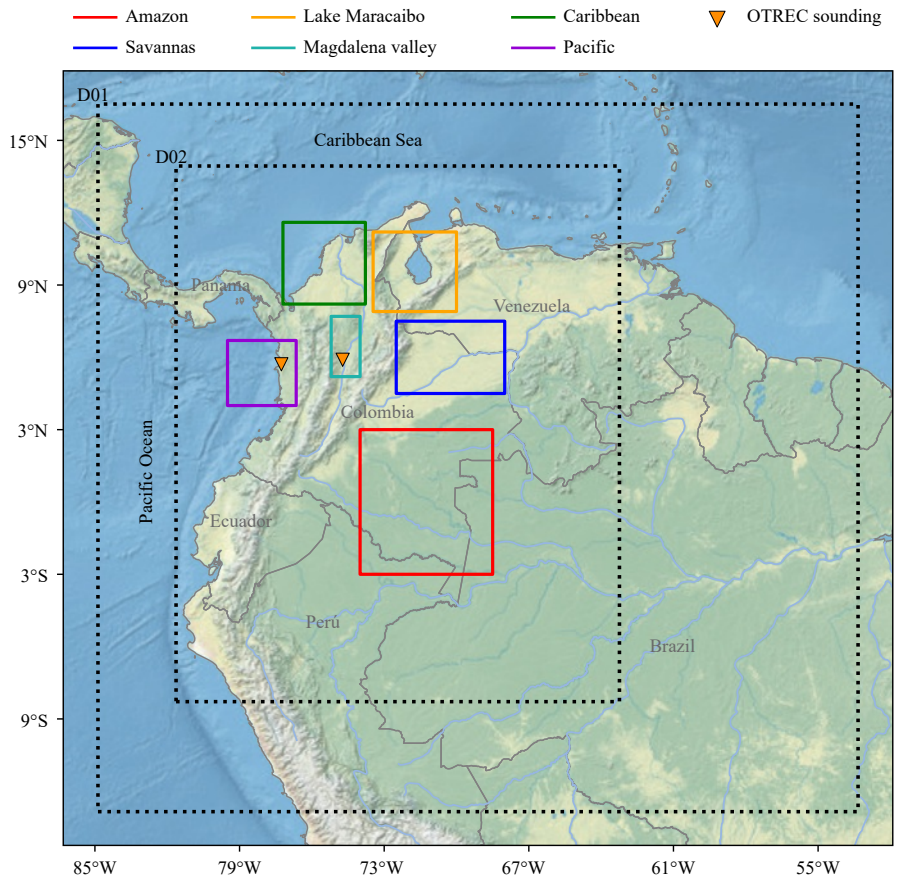

Fig. 1. Study region and domains of the WRF simulations. Colored squares show the regions and orange triangles the location of OTREC soundings launched during the study period.

ted) strategy with a resolution of 12 km in the external domain (parameterized convection) and 4 km in the inner domain (convection-permitting), where all the analyses were focused. Simulations were initialized with the fifth-generation ECMWF Reanalysis (ERA5) with a spatial resolution of 0.25°, and with boundary conditions updated every 3 hours. Sixty-five vertical levels were considered, and the time step was set to 48 s in the external domain. Additional details of the model configuration are found in Table 1.

Figure 1 shows the spatial extent of the domains. The outer domain covers northern South America, attempting to capture large-scale winds at low and medium levels, humidity fluxes from the Atlantic, and moisture from terrestrial evapotranspiration, identified as important moisture sources in the region (Sakamoto et al., 2011; Hoyos et al., 2018; Ruiz-Vásquez et al., 2020; Escobar et al., 2022). This domain also contains the regions where the three previously mentioned LLJs occur. The inner domain covers Colombia, Ecuador, and most of Panama and Venezuela, as well as northern Peru, the upper part of the Brazilian Amazon basin, and the six regions described in Section 2.1.

Table 1. Summary of the WRF configuration for the performed simulations

Model parameter	Domain 1	Domain 2
Domain size	292 × 275	511 × 622
Grid size	12 km	4 km
Vertical level	65	65
Initial condition	ERA5	ERA5
Boundary condition	ERA5	Domain 1
	Physical parameterization	
Microphysics	WSM6	WSM6
	Thompson	Thompson
	Morrison	Morrison
Planetary boundary layer	YSU	YSU
	MYNN level 2.5	MYNN level 2.5
Cumulus	New Tiedtke	Off
Surface layer	Noah-MP	Noah-MP
Shortwave radiation	Dudhia	Dudhia
Longwave radiation	RRTM	RRTM

Three MP and two PBL parameterization schemes were used to analyze the rainfall sensitivity, representing a total of six WRF simulations. For MP, the implemented schemes were the WRF Single-Moment 6-class scheme (WSM6; Hong et al., 2006a), which considers six different types of hydrometeors and simulates the mixing ratio of these species (single-moment); the Thompson scheme (THOM; Thompson et al., 2008) that predicts the

mixing ratio for 6-class hydrometeors and number concentrations (double-moment) for ice and rain; and the Morrison double-moment scheme (MORR; Morrison et al., 2009), which predicts the mixing ratio of 6-class hydrometeors, and number concentrations for ice, snow, rain, and graupel. For PBL, the two schemes implemented were the Yonsei University (YSU; Hong et al., 2006b) and the Mellor–Yamada Nakanishi Niino level 2.5 (MYNN; Nakanishi and Niino, 2006; Olson et al., 2019). YSU is a non-local first-order closure PBL scheme that includes an explicit treatment of entrainment in the PBL top. Non-local mixing in this scheme is represented using a counter-gradient term in the diffusion equation. On the other hand, MYNN is a 1.5-order TKE-based closure scheme with closure constants based on results of Large Eddy Simulations (LES). MYNN also includes a partial condensation approach to account for the effects of subgrid-scale clouds on the turbulent fluxes. In recent WRF versions, an eddy-diffusivity mass-flux approach is also used to account for non-local mixing in the PBL (Olson et al., 2019). Despite having differences in the level of complexity, these schemes are well known for providing good results in other regions (Tian et al., 2017; Reshmi Mohan et al., 2018; Yáñez-Morroni et al., 2018; Gbode et al., 2019; Martínez-Castro et al., 2019). The rest of the setup includes the New Tiedtke cumulus scheme (only in Domain 1; Zhang and Wang, 2017), the revised MM5 (fifth-generation mesoscale model) surface layer scheme (Jiménez et al., 2012), the Noah-MP land-surface model (Niu et al., 2011), the Dudhia (Dudhia, 1989) shortwave radiation scheme, and the Rapid Radiative Transfer Model (RRTM; Mlawer et al., 1997) for longwave radiation.

2.3 *Model evaluation*

Model evaluation was based on satellite information, covering the whole region at high temporal resolution. The IMERG (integrated multi-satellite retrievals for GPM) Final Run product from the Global Precipitation Measurement (GPM) satellite network was used to evaluate the simulated rainfall due to its high spatial (0.1°) and temporal (30 min) resolutions (NASA, 2019). Also, for completeness, we included precipitation measurements from the Institute of Hydrology, Meteorology and Environmental Studies (IDEAM) and Corantioquia (Piragua network) rain gauges. However, the evaluation was not focused on this information due to its limited spatial coverage (the network is focused on populated areas), and the type of evaluation metrics implemented (described below). Additionally, given the relationship between vertical cloud development and low brightness temperature (BT) values, we assessed the model's ability to simulate deep convective clouds using the BT information from MERGIR (NASA, 2017), which merges data from geostationary satellites worldwide at spatial and temporal resolutions of 4 km and 30 min, respectively.

Furthermore, soundings from the OTREC project were also included in the evaluation of vertical profiles from 0000 UTC 19 to 0000 UTC 24 September. These soundings contain valuable information about atmospheric dynamics and thermodynamics, useful to evaluate the simulations. Specifically, profiles of zonal and meridional winds, relative humidity, and equivalent potential temperature were used for the comparison with the simulations. Information from soundings is available twice a day (0000 and 1200 UTC) from two locations: Nuquí on the Colombian Pacific coast (5.71°N, 77.27°W) and Puerto Triunfo in the Magdalena valley (5.9°N, 74.72°W). Additional soundings were launched at 0600 and 1800 UTC during days of intense operation periods. Fuchs-Stone et al. (2020) and Mejía and Poveda (2020) described the OTREC field campaign in more detail.

We used different metrics to evaluate the performance of the simulations. We linearly interpolated WRF and satellite fields to a common grid with a 12-km × 12-km spatial resolution. First, we applied traditional verification metrics based on 2 × 2 contingency tables to the precipitation fields (Wilks, 2011). In these methods, a table is created using the number of times the model captures whether or not rainfall will overcome a certain percentile (an event). Several skill metrics can be computed by using this strategy, including the probability of detection (POD), false alarm ratio (FAR), and critical success index (CSI). Particularly, the CSI (also known as Threat Score) accounts for the model's ability to represent observed events relative to the times that the event was both simulated and observed. It accounts not only for the number of successes but also those relative to the errors. The CSI method for a given pixel and the whole study period was calculated in Eq. (1), where hits (Hi) are observed events simulated by the model, false alarms (Fa) are simulated but not observed events, and misses (Mi) are observed events that were not simulated.

$$\mathrm{CSI} = \frac{\mathrm{Hi}}{\mathrm{Hi} - \mathrm{Fa} - \mathrm{Mi}}. \tag{1}$$

Traditional evaluation metrics use a pixel-to-pixel strategy, which penalizes small spatial biases in the model. Metrics such as the Fractions Skill Score (FSS; Roberts and Lean, 2008) were developed to overcome this issue. The FSS compares the ratio of pixels that exceed a threshold in the model and observations in a spatial rolling window for a given time step, avoiding double penalties. A variation of the original skill metric called

Localized FSS (LFSS; Woodhams et al., 2018) was used here, which is similar to the original but allows representing the spatial performance of the model, helping to describe differences by region. Equation (2) details the procedure to calculate the LFSS. The metric was computed for a neighborhood centered in the pixel *i, j* and averaged over *k* time steps. The numerator on the right-hand of Eq. (2) is the mean squared error (MSE) of the number of pixels exceeding the threshold in observation $F_{o,i,j,k}$ and simulations $F_{s,i,j,k}$, while the denominator represents a low-skill MSE, which is used as a reference.

$$\mathrm{LFSS}_{i,j} = 1 - \frac{\sum_{k=1}^{n}\left(F_{o,i,j,k} - F_{s,i,j,k}\right)^2}{\sum_{k=1}^{n}\left(F_{o,i,j,k}^2 + F_{s,i,j,k}^2\right)}. \quad (2)$$

3. Results

The results section is divided into two parts. First, we present the evaluation of the different MP and PBL simulations, describing the main differences among the schemes. Subsequently, we analyze processes that can explain the sensitivity to MP and PBL parameterizations in specific regions.

3.1 *Model evaluation*

Figure 2 shows the mean spatial distribution of rainfall during the study period for both observations and simulations. GPM-derived rainfall (upper left panel) indicates higher precipitation rates to the west of Colombia (Pacific region) and to the north of the domain (Lake Maracaibo and Magdalena valley), with less and more scattered rain over other regions. Similarly, rain gauges (lower left panel) exhibit more rainfall in the northwest and less over the Andes Mountain range, with some differences regarding satellite data. These differences occur as the rain gauge network is more dense in the Andean zone and also constrained to continental areas, which does not allow capturing the main rainfall hotspots evidenced in the Colombian Pacific and the Maracaibo Lake. Nevertheless, it is noteworthy that satellite information is useful for capturing the spatiotemporal variability of rainfall and evaluating the performance of the simulations. In general, the simulations represented the main features of the spatial distribution of rainfall in the different regions. However, compared to observations, the model overestimated the precipitation magnitude, especially towards the north and west of the country.

MP and PBL parameterization schemes exhibited notable differences in the simulated rainfall fields. In relation to PBL, the simulations performed with YSU resulted in more precipitation, notably in the Savannas and Amazon regions, as well as in northern Perú. In relation

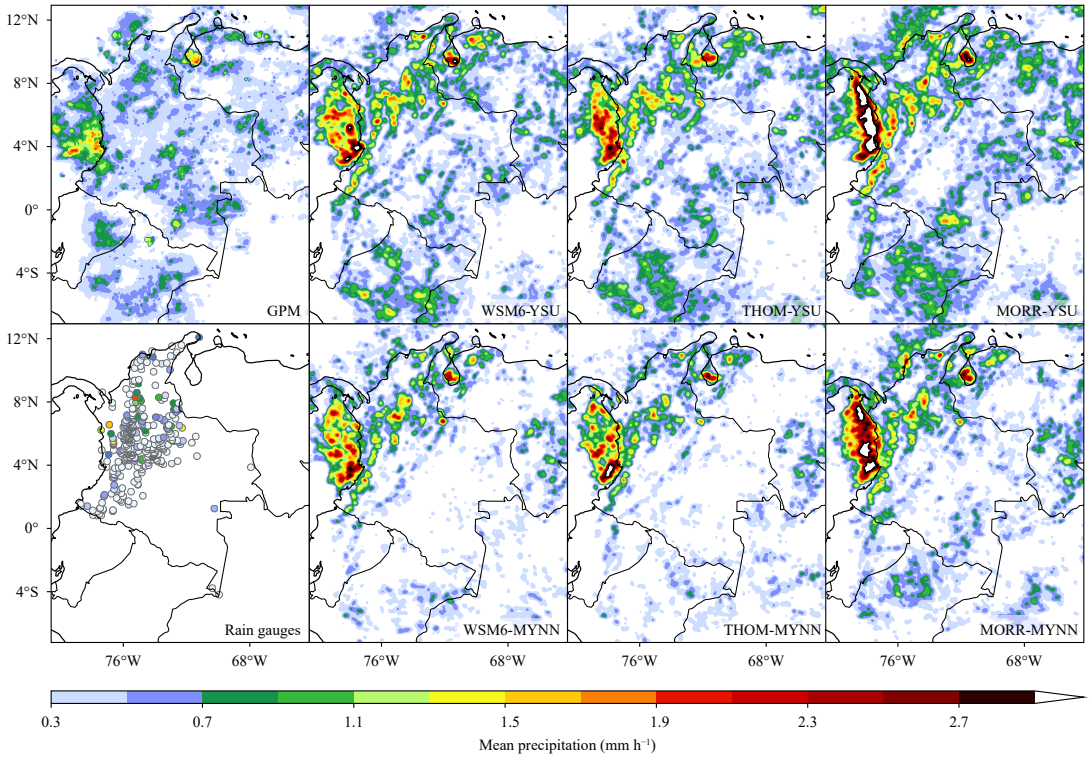

Fig. 2. Spatial distributions of mean precipitation during the study period for the whole region. Satellite information (GPM) and rain gauges (IDEAM and Piragua) are depicted on the left panels of the figure, followed by the results of the WRF simulations. Parameterization schemes were plotted as a function of their complexity.

to MP, MORR shows more rainfall in general, but there is an especially large overestimation in the Pacific region, while WSM6 and THOM are closer to observations and correctly allocated the maximum to the south of the Colombian Pacific coast. Particularly, WSM6 produces a rain patch further from the coastline than THOM and MORR, indicative of the offshore propagation of convective systems in the region (Mejía et al., 2021).

Time series of cumulative rainfall are presented in Fig. 3 for the six regions. Satellite precipitation showed a similar variability to that from rain gauges, with some differences in magnitude in certain regions. Of note is that the number of stations and the area coverage of rain gauges are limited, and thus time series derived from gauges are not directly comparable to model or satellite-derived data (Urrea et al., 2019; Vallejo-Bernal et al., 2021; Valencia et al., 2023). Simulations captured the occurrence of most rainfall events during the study period, with differences in intensity. In particular, the model overestimated precipitation in regions influenced by mountains, such as Maracaibo, Magdalena valley, Caribbean, and Pacific. At the same time, cumulative rainfall was underestimated in regions where orography is relatively flat, such as Savannas–Amazon. In NWSA, the overestimation of precipitation in convection-permitting simulations was previously reported in topographically-influenced regions such as the Magdalena valley (Gomez-Rios et al., 2023). However, the underestimation in mostly flat regions such as the Amazon–Savannas had yet to be reported previously, as these regions have been less studied.

Cumulative rainfall was largely affected by the MP and PBL schemes in the six regions (Fig. 3). First, simulations using the MYNN local PBL scheme (dashed lines) produced less rain in the six regions, with the largest difference in the Amazon–Savannas regions (around 25 mm). As a result, simulations with MYNN underestimate rainfall in the Amazon–Savannas flatlands, while YSU better agreed with observations. Similarly, MP schemes remarkably influenced the amount of rainfall, with MORR producing more rainfall in the six regions. Particularly, MORR had a larger overestimation in regions westward of the Andes such as the Caribbean (differences up to 40 mm) and Pacific (differences up to 90 mm).

Figure 4 shows the CSI for the performed simulations and computed for different thresholds (percentiles). There is no generalized behavior in the performance of the simulations, as some schemes demonstrated better performance in some regions while other schemes per-

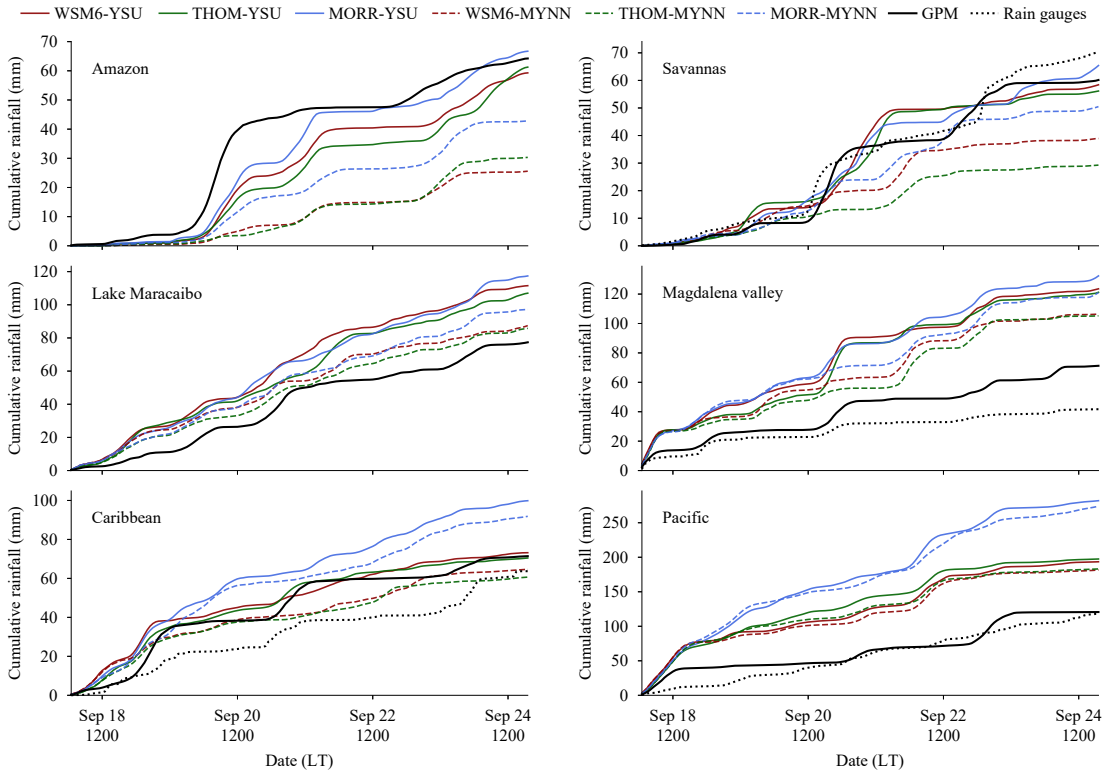

Fig. 3. Cumulative rainfall during the study period averaged for each of the six different regions. Black lines show satellite-based rainfall (GPM), dashed black lines represent gauge-based rainfall, and colored lines are the simulated rainfall using different schemes. Only one rain gauge was available in the Amazon region, so it was not included. LT: local time.

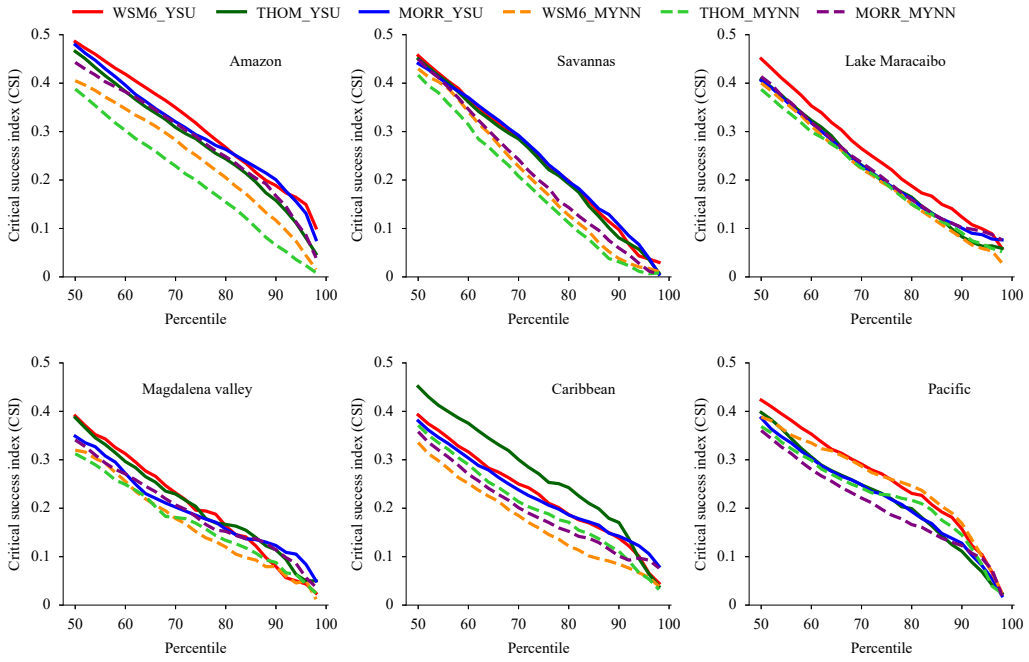

Fig. 4. Critical success index (CSI), also called threat score, computed as a function of a rainfall percentile. Values were calculated for each of the six regions (panels) and parameterization schemes (colored lines). Higher values indicate better performance.

formed better in others. However, the simulations performed with WSM6 and YSU showed good performance in the regions, being superior or similar to other schemes, except for the Caribbean, where THOM–YSU had the highest CSI.

Assessing the representation of deep convection is relevant due to its relationship with extreme rainfall events. Figure 5 presents the LFSS for BT in the study area. Simulations with MORR had issues reproducing the spatial distribution of BT, showing low LFSS for most of the model domain. WSM6 and THOM performed similarly with better results in Maracaibo, the Pacific, and the Caribbean, and poorer results in the Savannas and Amazon. THOM outperformed WSM6 in the Caribbean, while WSM6 performed better in the inter-Andean Magdalena valley. Consistent with precipitation results, MYNN simulations performed worse than YSU for BT in the Amazon and Savannas regions.

In order to check the model's capacity to represent the vertical behavior of dynamic and thermodynamic variables, an analysis with the OTREC soundings was performed. Figure 6 displays the average zonal and meridional wind profiles, relative humidity, and equivalent potential temperature for the two OTREC sounding sites (see Fig. 1). Additional assessment of the vertical and temporal variations of soundings can be found in Taylor diagrams of Supplementary Fig. S2. In general, the simulations captured the vertical variations of the variables, even though some differences between schemes were observed. In the Nuqui soundings (upper panels), winds below 900 hPa were mainly overestimated by the simulations for the zonal component, while simulations underestimated the meridional component, which means that the modeled winds are mostly westerly while observations also have a southerly component (southwesterly wind). MORR showed the best performance at low levels but had westerly winds at medium levels instead of easterlies and underestimated the easterly winds at high levels. The model adequately represented the high relative humidity from the surface to 400 hPa (> 80%) and the sharp decrease at high levels. However, simulations with WSM6 and THOM–MYNN underestimated humidity at higher levels, while MORR overestimated at medium levels. Additionally, the equivalent potential temperature in Nuquí showed lower values at low levels, while a higher temperature was observed for MORR at high levels, which may be related to deeper convection and consequently greater latent heat release at high levels for this scheme.

All the simulations in Puerto Triunfo overestimated low-level winds, especially for the up-valley component. THOM–YSU exhibited the closest similarity with observations. A low sensitivity between parameterizations was observed at medium levels, while WSM6 had a better performance at high levels. In addition, the relative humidity and the equivalent potential temperature presented a similar behavior to that described in Nuquí. Overestimations observed in the zonal winds (Nuquí soundings)

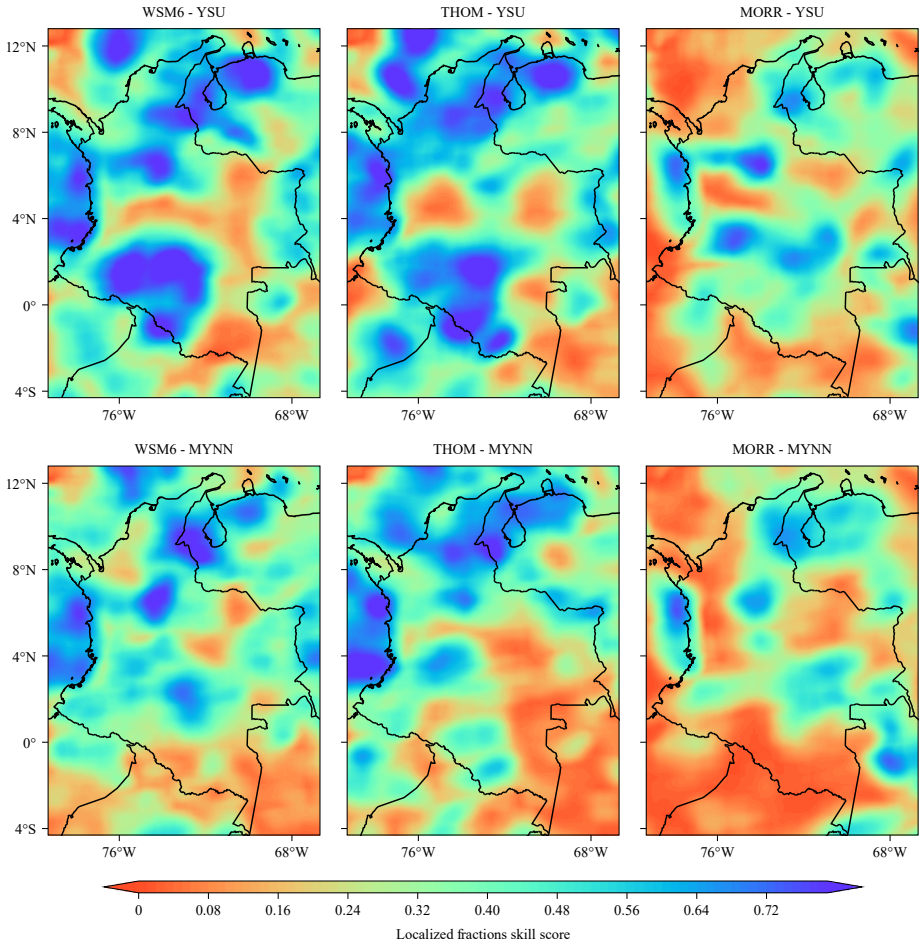

Fig. 5. Localized Fractions Skill Score (LFSS) computed for brightness temperature during the whole study period using the implemented parameterization schemes. Metrics are calculated by using a 40-pixels window and the 10th percentile is used as a threshold.

and up-valley winds (Puerto Triunfo soundings) are likely related to the rainfall overestimation in the Pacific and the Magdalena valley, respectively. This is due to the fact that zonal winds (related to the Choco LLJ) are essential to generate moist convection in the Pacific (Mejía et al., 2021; Riley Dellaripa et al., 2023), while up-valley winds transport moisture for convection in the Magdalena (Gomez-Rios et al., 2023).

3.2 *Analysis of atmospheric processes*

Identifying the processes that have greater sensitivity to the selection of MP and PBL schemes helps to elucidate the atmospheric mechanisms playing a fundamental role in the occurrence, magnitude, and intensity of rainfall in a particular region, which is crucial for developing and improving parameterizations in atmospheric models. This section analyzes processes impacting the precipitation sensitivity to MP and PBL parameterizations, emphasizing the regions with the most significant sensitivity. The Amazon region was selected to analyze processes that could be influencing sensitivity among PBL schemes and the Pacific for MP processes since there are more remarkable differences between PBL schemes in the Amazon-Orinoco flatlands (Supplementary Fig. S3) and between MP schemes on the Pacific coast (Supplementary Fig. S4), with average differences up to 1 mm h^{-1}. The simulations were averaged over MP schemes to isolate the sensitivity associated with PBL schemes. Similarly, the average over PBL schemes was carried out to study the sensitivity to MP schemes.

3.2.1 *Sensitivity to PBL*

Rainfall representation in the Colombian flatlands exhibited a larger sensitivity to the PBL schemes. As the Colombian Amazon is a region of high climatological, ecological, and hydrological importance, processes causing sensitivity between PBL schemes are studied in detail. Low-level processes have been previously identified as drivers of convection and precipitation in the Amazon-Orinoco flatlands (Martínez et al., 2022). Figure 7 shows the mean lower tropospheric integrated moisture flux, its convergence, and mean 700-hPa vertical moisture flux for the two PBL schemes. Simulations with YSU, which

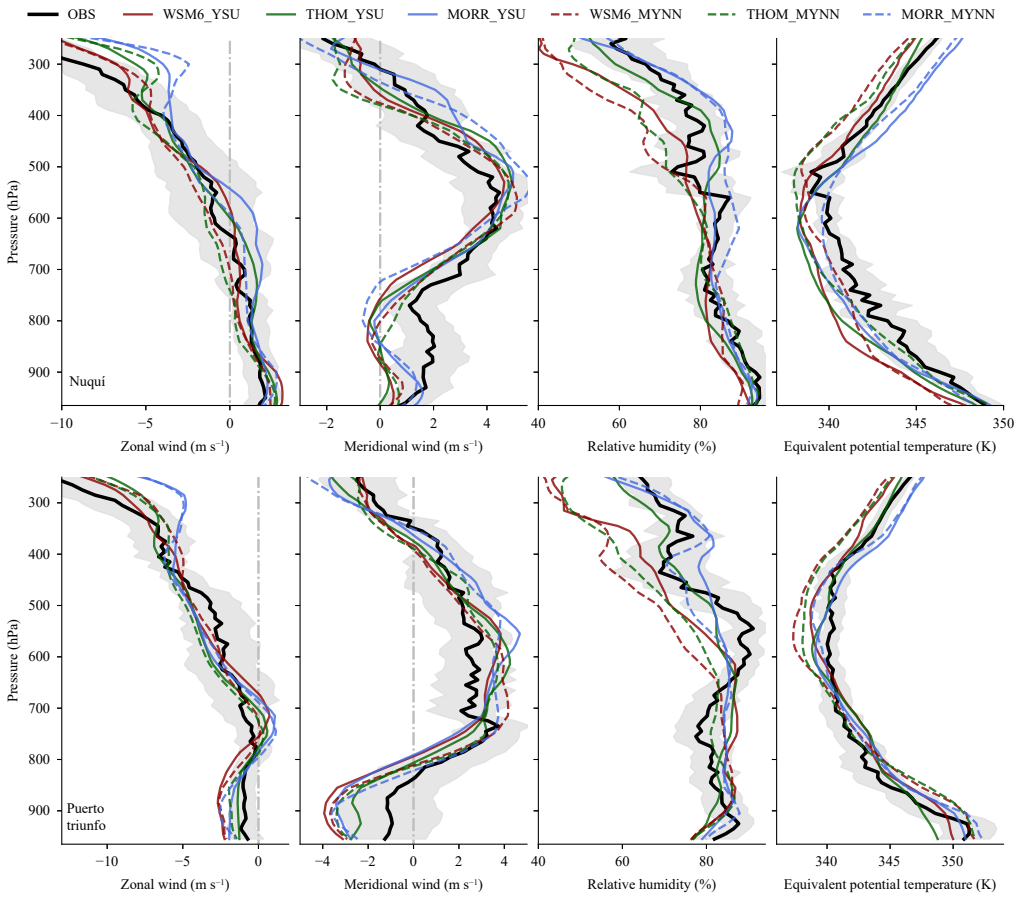

Fig. 6. Profiles of dynamic and thermodynamic variables for the radiosondes released in Nuquí (upper panels) and Puerto Triunfo (lower panels). The black line denotes the values measured by the radiosondes with the standard deviation shaded in gray, and the colored lines show the values simulated by each of the experiments. From right to left are the zonal wind, meridional wind, relative humidity, and equivalent potential temperature. The launch locations for the soundings are specified in Fig. 1.

previously showed higher rain rates, exhibited enhanced moisture flux from the southeast (left-hand panels), which flows from the Amazon rainforest into the Colombian Amazon. Besides, a notable decrease in low-level moisture flux for YSU (orange to red colors) coincides with greater moisture convergence (colored contours in the right figures) over the Colombian Amazon. Moisture convergence patterns resulted in stronger wet convection for YSU than for MYNN (gray contours in right panels) over the entire region of interest, favoring deep cloud formation and precipitation occurrence.

Energy and moisture fluxes from the earth's surface, which are critical factors in determining wet convection and rainfall occurrence, are widely influenced by PBL schemes. Figure 8 shows the mean daytime simulated sensible and latent heat fluxes and the incoming shortwave radiation at the surface. Compared to MYNN, greater sensible and latent heat fluxes were obtained in the simulations with YSU, with differences of 30% for sensible heat and 20% for latent heat in the Colombian Amazon region (delimited by the rectangle in Fig. 8). The incident shortwave radiation was also higher in YSU with differences over 100 W m^{-2}. An initial assessment showed that downward longwave radiation is similar between both PBL schemes (figure omitted). These results suggest that differences in heat fluxes are mainly associated with the differential entrance of solar radiation at the surface between the two PBL schemes rather than direct differences in the simulated fluxes. As a result of the increased heat fluxes, the YSU-simulated atmosphere has more energy and moisture to enhance horizontal and vertical humidity transport (Fig. 7), and thus trigger deep convection. Notably, although YSU showed higher precipitation, it did not result in a reduction of the incident radiation, suggesting that the vertical distribution of clouds plays an important role in the differences between the schemes.

To explain the observed differences in incident shortwave radiation and the sensible and latent heat fluxes, Fig. 9 shows the diurnal variability of cloud fraction at different levels. MYNN produced a higher cloud fraction at low levels (between 1000 and 4000 m asl) than

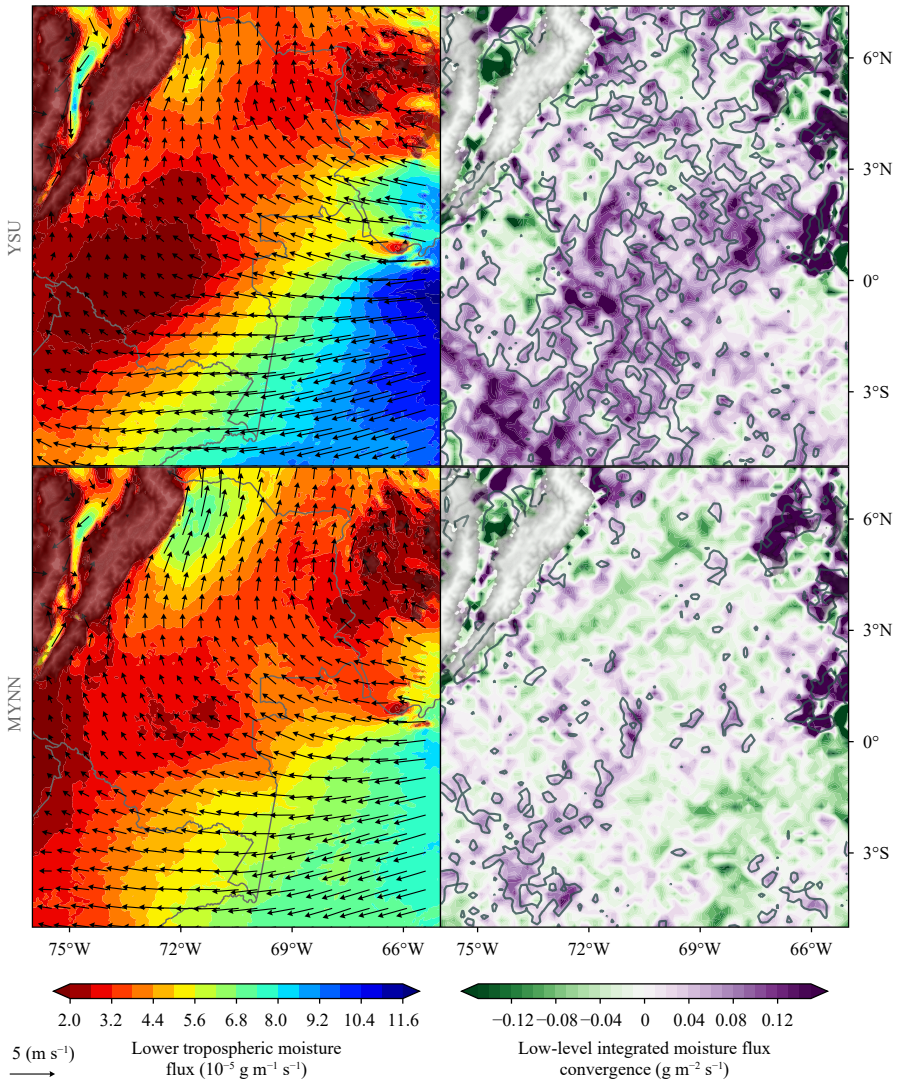

Fig. 7. Magnitude of mean lower tropospheric (1000–800 hPa) moisture flux (colored contours) and horizontal winds at 850 hPa (arrows) in the left panels, and mean lower tropospheric moisture flux convergence (colored contours) and 0.05-g kg^{-1} m s^{-1} vertical moisture flux at 700 hPa (gray contours) in the right panels.

YSU, especially during hours with high solar activity (between 0900 and 1500 LT). Low-level clouds (especially stratus and stratocumulus) are known to have high optical depths and a high albedo, producing a net surface cooling effect (Oreopoulos et al., 2017; L'Ecuyer et al., 2019). In this sense, higher amounts of low-level clouds in MYNN could decrease sensible and latent heat fluxes. Furthermore, a possible positive feedback can be inferred in MYNN, where the presence of low-level clouds decreases the incident shortwave radiation and turbulent heat fluxes, causing shallower convection than YSU, and producing more lower clouds, which in turn reduces heat fluxes. On the other hand, YSU exhibited a higher fraction of mid-level clouds, which can be associated with deeper convection and precipitation. At high levels, no marked differences were identified between the PBL schemes, which coincides with similar results for downward longwave radiation between YSU and MYNN (figure omitted).

Furthermore, an additional simulation was performed to explore the causes of the differences in the simulated low-level cloud fraction and its interaction with radiation (see Supplementary Fig. S1 and Table S1). The MYNN scheme includes a representation of sub-grid scale (SGS) clouds in the boundary layer that are also coupled to the longwave and shortwave radiation schemes (Olson et al., 2019). Hence, the rationale behind the new simulation is to test the sensitivity of the SGS clouds by turning off their representation in MYNN (icloud_bl = 0). The new simulation exhibited a significant reduction in the low-level cloud fraction and an increase in incident shortwave radiation and surface turbu-

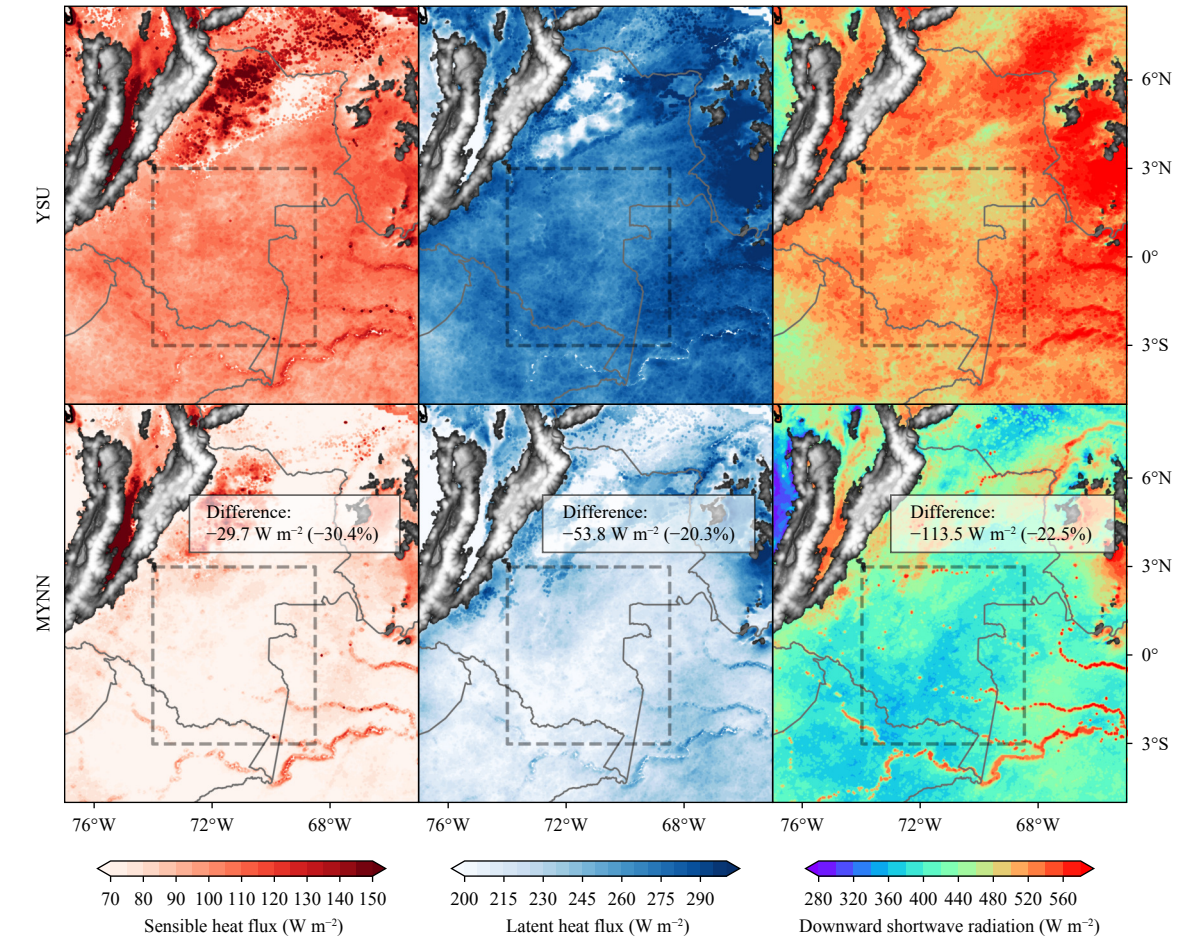

Fig. 8. Mean daytime (0700–1700 LT) sensible heat (left columns), latent heat (middle columns), and downward shortwave radiation (right columns) as simulated by YSU (upper panels) and MYNN (lower panels) simulations. Annotations in lower panels show the absolute and percentage differences between schemes (MYNN minus YSU) in the Colombian Amazon (delimited region).

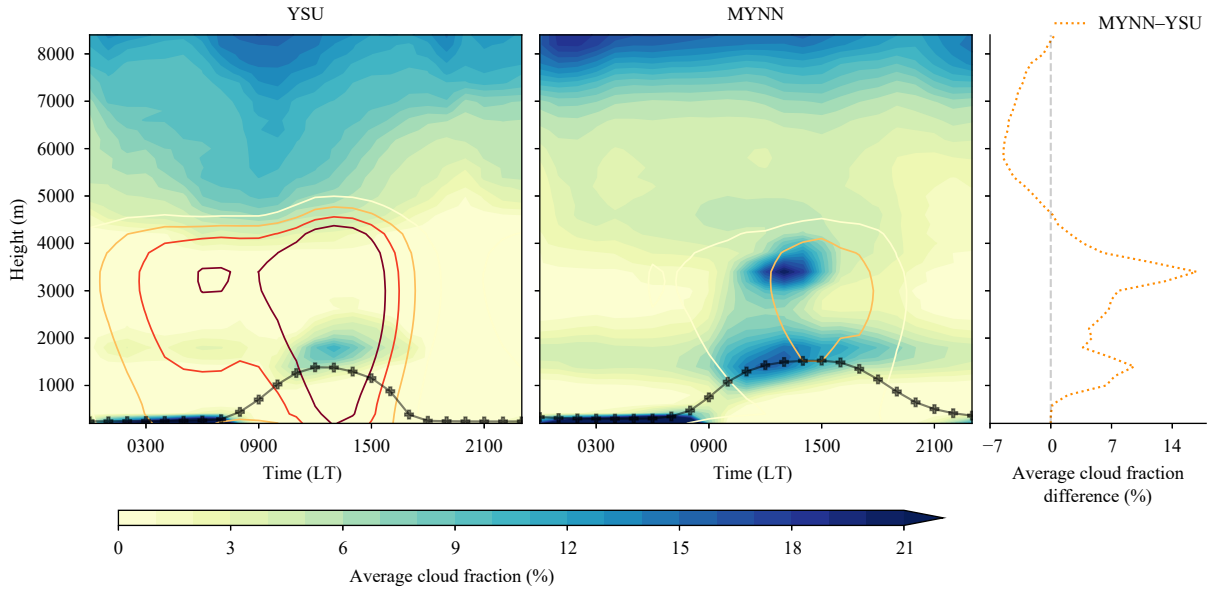

Fig. 9. Daytime–height distributions of cloud fraction (filled contours) averaged during the study period and over the defined Colombian Amazon region. The diurnal cycle of the planetary boundary layer height (PBLH) is depicted by the gray line. Yellow to red contours represent the rainwater mixing ratio. The right panel shows the difference between the cloud fraction profile from 1000 to 1400 LT.

lent fluxes (Supplementary Table S1), suggesting that this parameter is determinant for the adequate simulation of clouds and radiation, and helps to explain the differences between PBL schemes.

3.2.2 *Sensitivity to microphysics*

As previously described, rainfall sensitivity to MP schemes is larger in western Colombia, along and offshore the Pacific coast (also shown in Supplementary Fig. S4). Here, an analysis of processes causing this sensitivity is carried out. Figure 10 presents the evolution of lower tropospheric integrated moisture flux and the vertical moisture flux along the day, averaged over latitudes across the Pacific region defined in Fig. 1. Surprisingly, remarkable differences in moisture transport are observed among MP schemes. First, WSM6 and THOM showed similar low-level moisture flux patterns (left panels) with enhanced transport toward the continent between 1400 and 2000 LT, producing moist convection in the western foothills of the Andes (around 76.5°W; right panels). Afterward, convection develops in the ocean during the early night and the morning. By contrast, MORR showed a more intense and longitudinally exten-

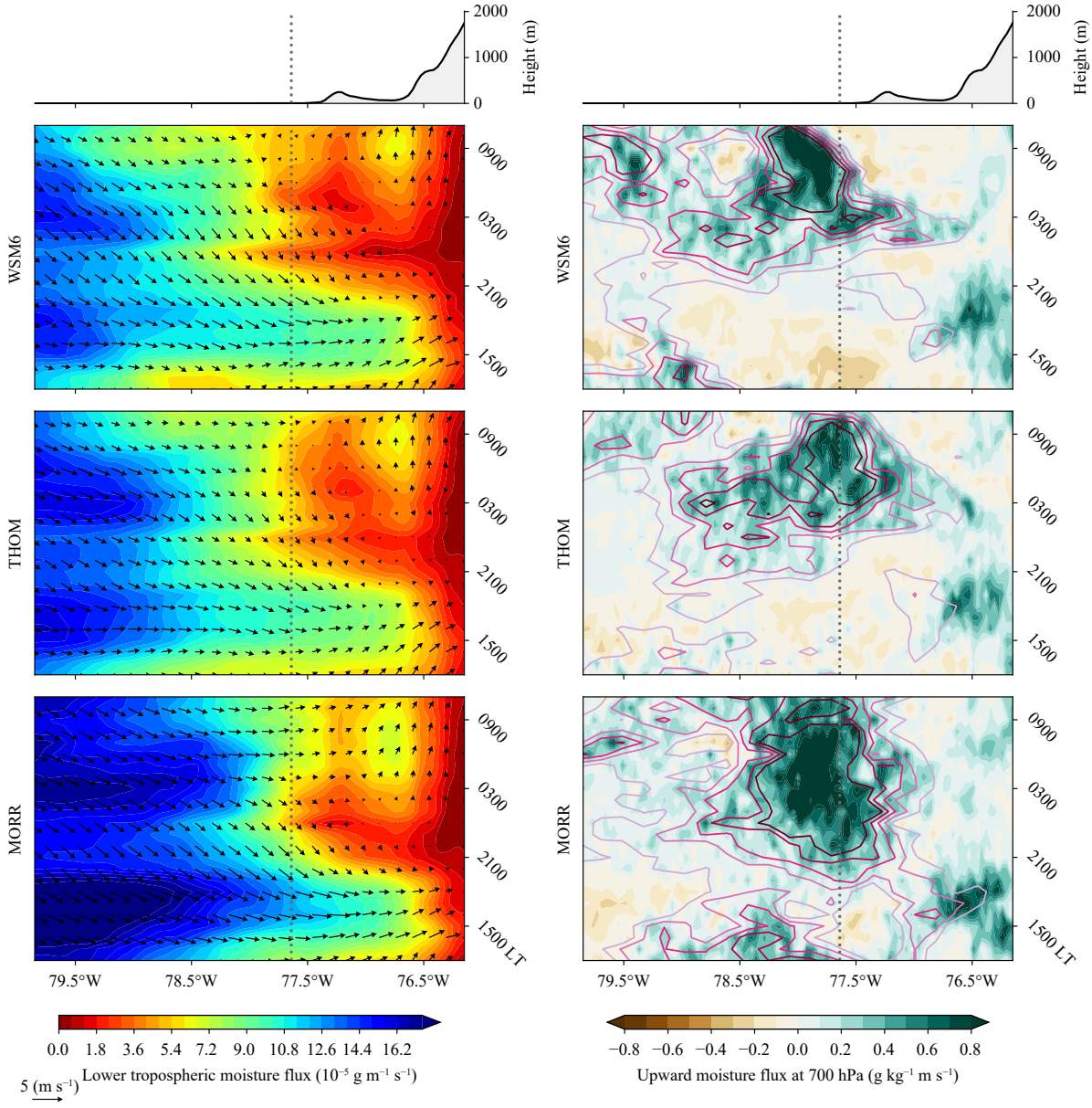

Fig. 10. Mean diurnal and longitudinal moisture flux integrated from 1000 to 800 hPa (left panels) and vertical moisture flux at 700 hPa (right panels). The convergence of lower tropospheric moisture flux is represented as purple contours in the right-side panels and arrows in the left panels show 850-hPa horizontal winds. Mean topography is indicated at the top of the figure. Values were averaged latitudinally for the Pacific region delimited in Fig. 1.

ded low-level moisture flux throughout the day. Consequently, convection in MORR was more intense and long-lasting than in WSM6 and THOM. These results show that selecting MP schemes in the Pacific impacts low-level and vertical moisture fluxes, which are relevant factors for rainfall development and moist convection in the region (Mejía et al., 2021; Riley Dellaripa et al., 2023).

Figure 11 shows the longitude–height section of vertical and zonal winds and the diabatic heating for the Pacific region to elucidate how MP schemes modify vertical fluxes. MP parameterizations had a marked impact on convection in the Pacific, with large differences among schemes. As in the previous figure, WSM6 and THOM showed similar patterns, with convection near the shoreline from 900 to 600 hPa and a broader convective region aloft. However, the convective structure in WSM6 was more intense and further offshore, consistent with the rainfall patterns (Fig. 2). Contrarily, MORR exposed a broader convective region with stronger convection and a greater amount of rain generated near the shoreline (77.5°–78.5°W). This result indicates that the MP para-

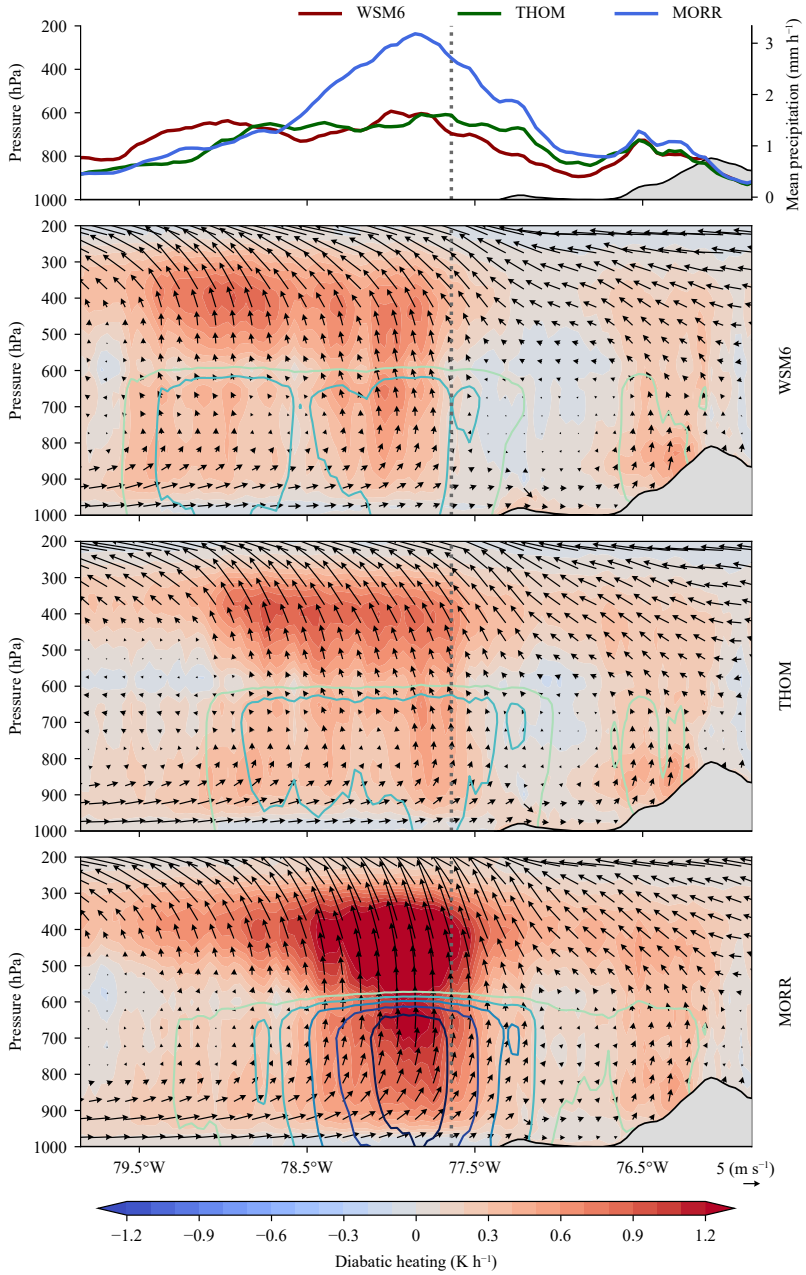

Fig. 11. Longitude–height section of mean vertical and zonal winds (arrows) and diabatic heating (colored contours). Yellow to blue contours represent the rain mixing ratio. Note that vertical winds were multiplied by 100 in order to improve representation. The section was averaged latitudinally for the Pacific region delimited in Fig. 1.

meterization schemes notably affect the intensity and location of convection in the Pacific region, which can influence low-level humidity fluxes and convergence by mass continuity. Moreover, sources and sinks of heat are represented by diabatic heating in Fig. 11. MORR released large amounts of heat at medium–high levels (500–300 hPa), producing a more intense top-heavy diabatic heating profile compared to WSM6 and THOM.

Water phase changes act as sources and sinks of heat to the atmosphere. In order to compare the latent heat release by the MP schemes, Fig. 12 shows the mixing ratio for different hydrometeor species. Notable differences

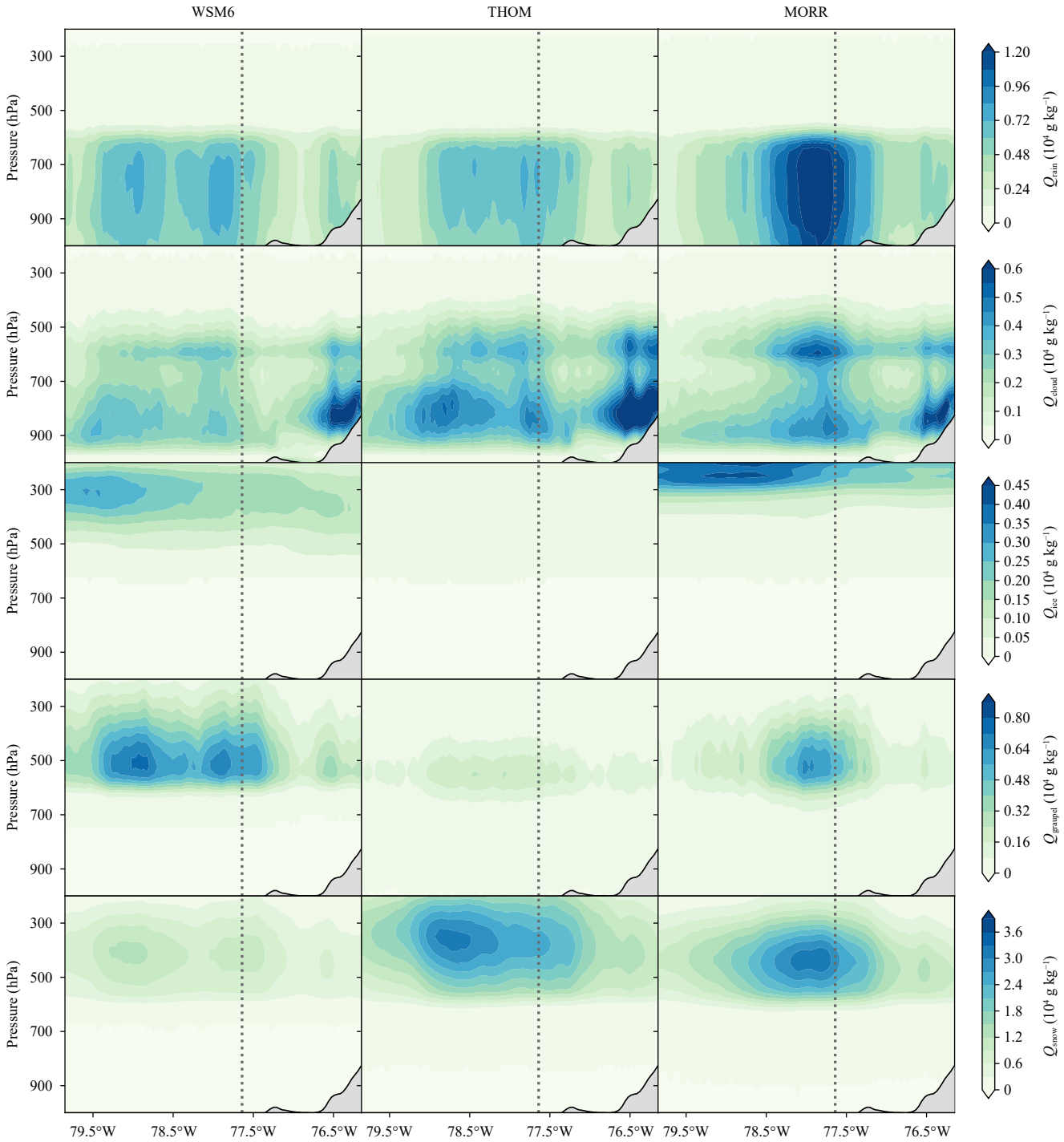

Fig. 12. Longitude–height section of averaged mixing ratio for different species of hydrometeors. From left to right: WSM6, THOM, MORR. From top to bottom: mixing ratio for rain, cloud, ice, graupel, and snow species. The section was averaged latitudinally for the Pacific region delimited in Fig. 1.

were observed in the solid phase hydrometeors. WSM6 featured graupel around 500 hPa and ice aloft, with both extending and reaching a maximum in the oceanic region. In contrast, THOM produced a large amount of snow between 500 and 300 hPa, which extends into the ocean, although not as far as WSM6. Conversely, MORR showed the presence of the three solid-phase hydrometeors (ice, graupel, and snow), with graupel and snow much closer to the shoreline than WSM6 and THOM, while the ice was produced above 300 hPa with a much higher mixing ratio than WSM6 and more extended into the oceanic region as well. In the MORR simulations, ice nucleation could be favored by water below the freezing point (supercooled liquid water) above 600 hPa. Furthermore, graupel production by riming could be favored in the mixed-phase region allocated between 600 and 400 hPa. These processes imply phase changes from liquid to solid and vapor to solid and a subsequent release of latent heat, which could explain the greater diabatic heating observed in MORR. The possible implications of these results are discussed below.

4. Conclusions and discussion

This work studied the sensitivity of precipitation to the selection of PBL and MP schemes in northwestern South America, including an analysis of processes behind rainfall representation. Simulations were performed with the WRF model using three MP schemes (WSM6, THOM, and MORR) and two PBL schemes (YSU and MYNN), and the model evaluation was based on satellite information and soundings.

We found that the model overestimated rainfall in regions with influence of topographic features, such as Maracaibo, Magdalena valley, the Caribbean, and the Pacific, while underestimated over the Savannas–Amazon where orography is relatively flat. In general, simulations captured the spatiotemporal rainfall characteristics during the study period, as well as the vertical profiles of dynamic and thermodynamic variables. Although the performance was highly dependent on the study region, the less computationally expensive WSM6 and THOM provided the best results among the MP schemes, while the YSU PBL scheme performed better than MYNN. Other studies have evidenced better results for less computationally expensive MP and PBL parameterization schemes, which are essential for forecasting tasks. For example, despite a single-moment MP scheme, WSM6 has shown good results in simulating rainfall events (Tian et al., 2017; Yáñez-Morroni et al., 2018; Huang et al., 2020; Liu et al., 2020). Likewise, THOM has shown better results than more complex schemes such as MORR (Karki et al., 2018; Reshmi Mohan et al., 2018). For PBL, the non-local scheme YSU has shown better results than local schemes like MYNN (Efstathiou et al., 2013; Tian et al., 2017; Comin et al., 2021; Prein et al., 2022; Zhu et al., 2022), which is computationally more expensive.

Nevertheless, it is important to highlight that distinct tunable parameters that were not adjusted during the study can generate large uncertainties in the parameterization schemes (Yang et al., 2019), impacting the performance of the schemes. Recent studies have performed modified experiments to improve the performance of PBL (Yang et al., 2019; Hu et al., 2023) and MP (Halder et al., 2015) schemes. More field campaigns would be beneficial to adequately adjust these parameters and improve simulations in poorly monitored regions such as the NWSA.

Simulations using the YSU PBL scheme produced higher rainfall rates, especially in the Amazon–Orinoco flatlands, whereas MYNN underestimated rainfall. Previous sensitivity analyses in different regions have highlighted that non-local PBL schemes generate greater mixing and precipitation than local schemes (Efstathiou et al., 2013; Que et al., 2016; Comin et al., 2021; Zhu et al., 2022). For instance, Efstathiou et al. (2013) showed that the vertical mixing produced by the local MYNN scheme was lower, diminishing the water vapor transport to higher levels, and thus causing lower precipitation rates than YSU. Also, Zhu et al. (2022) showed that MYNN produced less precipitation compared to YSU related to heavy rainfall generated by the passage of a tropical cyclone due to less vertical mixing for MYNN compared to YSU. In agreement with our work, different sensitivity analyses to PBL schemes in tropical South America have shown that simulations with YSU result in greater precipitation (Comin et al., 2021; Martínez et al., 2022; Prein et al., 2022; Hu et al., 2023). Although most of these studies showed better representation by YSU in the Amazon, Hu et al. (2023) reported a strong overestimation using this scheme, which differs from our findings. In this sense, our study provides additional elements for the discussion about which PBL schemes work best in South America.

Since PBL parameterizations strongly impact precipitation rates in the Amazon–Orinoco flatlands, processes related to these differences were studied in the Colombian Amazon. We found that the PBL schemes impact the incident solar radiation through variations in the vertical distribution of cloudiness. Specifically, MYNN produced a greater amount of low-level clouds, limiting the

incident solar radiation. Hu et al. (2023) found similar results when studying the sensitivity of PBL schemes in the Amazon, where the clouds simulated with the Asymmetric Convective Model v2 (ACM2) remained throughout the day while those simulated by YSU dissipated. These differences were attributed to moisture support from the free atmosphere in ACM2. In our case, the results showed that MYNN produces more low clouds (below 4000 m asl) instead of the mid-level clouds in Hu et al. (2023). An additional experiment showed that the enhanced production of low-level clouds in MYNN is associated with the representation of SGS PBL clouds and their coupling with radiation in this scheme (see Supplementary Fig. S5). In accordance with Min et al. (2022), this parameter (icloud_bl) notably affects the incoming shortwave radiation, which in turn influences heat fluxes and moist convection (see Supplementary Table S1). Prein et al. (2022) also showed that PBL schemes strongly impact cloudiness in the Amazon, with MYNN producing more cloudiness than YSU. As seen here, changes in incoming shortwave radiation associated with differences in the vertical cloud profile, impacted both sensible and latent heat fluxes, with the YSU scheme having higher values (differences in shortwave radiation and heat fluxes exceeding 20%). Similar to other recent studies (Wang et al., 2021; Martínez et al., 2022), the selection of the PBL had a marked influence on the low-level circulation, where YSU resulted in stronger moisture fluxes, convergence, and moist convection than MYNN, which can be associated with higher latent and sensible fluxes for YSU. Future studies should carefully consider how well PBL schemes represent cloudiness in the Amazon, given the high sensitivity it triggers in convective processes in the region.

On the other hand, MP schemes had less agreement in rainfall representation in the Pacific, with MORR producing much more rainfall than WSM6 and THOM. Specifically, MORR simulated a more marked upward moisture transport, which coincides with mid- to upper-level diabatic heating. Differences in simulated diabatic heating were mainly associated with the production of solid-phase hydrometeors in the mixed-phase zone. Previous studies have shown the importance of latent heat release in developing and maintaining convection. By modifying the ice-nucleation formulation in Morrison MP scheme, Halder et al. (2015) evidenced a greater release of latent heat in the upper atmosphere due to deposition, causing changes in the vertical wind speed. Huang et al. (2020) showed that MP schemes influenced convection development and propagation through differences in condensation-associated heating and evaporative cooling. Studying MCSs in the United States, Yang et al. (2017) and Feng et al. (2018) demonstrated the role of diabatic heating in producing feedbacks with the environment that influence circulation fields and the formation of a mesovortex, which contributes to forming more long-lived MCSs. Altogether, the findings of these studies coincide with the results presented here, suggesting that the release of latent heat caused by the formation of ice-phase hydrometeors may be influencing dynamic conditions, which are essential to determine convection and rainfall in the Pacific (Mejía et al., 2021).

MORR produced much more rainfall than THOM and WSM6, especially near the coastline, where we evidenced a higher production of snow and graupel in the mixed-phase cloud zone. Liu et al. (2021) showed that a greater availability of supercooled water droplets aided the development of snow and graupel, contributing to stronger rainfall, which is aligned with the behavior of MORR in the Pacific. Likewise, when studying the sensitivity of precipitation to MP schemes, Guo et al. (2019) and Jo et al. (2023) highlighted the contribution of graupel to the increase in rainfall, mainly due to melting. Future studies should consider a detailed microphysical budget (e.g., Shu et al., 2023) in the Colombian Pacific to unravel the origin of differences in simulated rainfall, as well as to elucidate possible mechanisms of convection organization in the region. Besides, MP schemes also modified the intensity and spatial structure of low-level moisture fluxes. Notably, MORR showed a Choco LLJ that extended deeper longitudinally than THOM and WSM6. Previous studies have also reported a significant impact of MP schemes on low-level moisture fluxes (Park et al., 2020; Podeti et al., 2020; Thomas et al., 2021). Specifically, Park et al. (2020) and Thomas et al. (2021) discuss the role of mid- to high-level latent heat release in convection intensity, which in turn influences low-level fluxes and convergence. Consequently, the stronger convection in MORR could explain the enhanced low-level moisture fluxes due to mass continuity. A discretized latent heat balance (Zhao et al., 2020) could contribute to better understanding the possible role of latent heat release in the dynamics of the Choco LLJ.

Finally, studies like this provide a framework that can contribute to the continuous improvement of parameterization schemes, which are fundamental for reducing the uncertainty of numerical models. As a first approach, it is important to point out that the study period is limited due to the computation cost of convection-permitting resolutions, and longer simulations could provide more robust conclusions. However, the modeling experiment, which sought to evaluate rainfall representation by different

parameterizations, to improve the understanding of the processes behind rainfall sensitivities and to be able to evaluate the results with the available soundings, provides valuable information for future studies. In addition, a more detailed assessment could include information from weather radars and surface stations. Future studies in this regard could be oriented in this direction.

Acknowledgments. The authors thank the three anonymous reviewers for providing valuable comments that greatly improved the original manuscript. IMERG and MERGE-IR satellite data were retrieved through NASA GES DISC server. ERA5 data were obtained from the Copernicus Climate Data Store. We thank IDEAM and Piragua for providing information from rain gauges, as well as the OTREC field campaign and the UNAL-MINCIENCIAS grant number 80740-128-2019 for providing the soundings.

Electronic supplementary material. Supplementary material is available in the online version of this article at https://doi.org/10.1007/s13351-024-3156-4 and is accessible for authorized users.

REFERENCES

Albrecht, R. I., S. J. Goodman, D. E. Buechler, et al., 2016: Where are the lightning hotspots on Earth? *Bull. Amer. Meteor. Soc.*, **97**, 2051–2068, doi: 10.1175/BAMS-D-14-00193.1.

Builes-Jaramillo, A., J. Yepes, and H. D. Salas, 2022: The Orinoco low-level jet and its association with the hydroclimatology of northern South America. *J. Hydrometeor.*, **23**, 209–223, doi: 10.1175/JHM-D-21-0073.1.

Chawla, I., K. K. Osuri, P. P. Mujumdar, et al., 2018: Assessment of the weather research and forecasting (WRF) model for simulation of extreme rainfall events in the upper Ganga Basin. *Hydrol. Earth Syst. Sci.*, **22**, 1095–1117, doi: 10.5194/hess-22-1095-2018.

Cohen, A. E., S. M. Cavallo, M. C. Coniglio, et al., 2015: A review of planetary boundary layer parameterization schemes and their sensitivity in simulating southeastern U.S. cold season severe weather environments. *Wea. Forecasting*, **30**, 591–612, doi: 10.1175/WAF-D-14-00105.1.

Comin, A. N., F. Justino, L. Pezzi, et al., 2021: Extreme rainfall event in the northeast coast of Brazil: A numerical sensitivity study. *Meteor. Atmos. Phys.*, **133**, 141–162, doi: 10.1007/s00703-020-00747-0.

Das, S. K., A. Hazra, S. M. Deshpande, et al., 2021: Investigation of cloud microphysical features during the passage of a tropical mesoscale convective system: Numerical simulations and X-band radar observations. *Pure Appl. Geophys.*, **178**, 185–204, doi: 10.1007/s00024-020-02622-w.

Dudhia, J., 1989: Numerical study of convection observed during the winter monsoon experiment using a mesoscale two-dimensional model. *J. Atmos. Sci.*, **46**, 3077–3107, doi: 10.1175/1520-0469(1989)046<3077:NSOCOD>2.0.CO;2.

Efstathiou, G. A., N. M. Zoumakis, D. Melas, et al., 2013: Sensitivity of WRF to boundary layer parameterizations in simulating a heavy rainfall event using different microphysical schemes. Effect on large-scale processes. *Atmos. Res.*, **132–133**, 125–143, doi: 10.1016/j.atmosres.2013.05.004.

Escobar, M., I. Hoyos, R. Nieto, et al., 2022: The importance of continental evaporation for precipitation in Colombia: A baseline combining observations from stable isotopes and modelling moisture trajectories. *Hydrol. Process.*, **36**, e14595, doi: 10.1002/hyp.14595.

Feng, Z., L. R. Leung, R. A. Jr. Houze, et al., 2018: Structure and evolution of mesoscale convective systems: Sensitivity to cloud microphysics in convection-permitting simulations over the United States. *J. Adv. Model. Earth Syst.*, **10**, 1470–1494, doi: 10.1029/2018MS001305.

Fuchs-Stone, Ž., D. J. Raymond, and S. Sentić, 2020: OTREC 2019: Convection over the East Pacific and Southwest Caribbean. *Geophys. Res. Lett.*, **47**, e2020GL087564, doi: 10.1029/2020GL087564.

Gbode, I. E., J. Dudhia, K. O. Ogunjobi, et al., 2019: Sensitivity of different physics schemes in the WRF model during a West African monsoon regime. *Theor. Appl. Climatol.*, **136**, 733–751, doi: 10.1007/s00704-018-2538-x.

Gomez-Rios, S., M. D. Zuluaga, and C. D. Hoyos, 2023: Orographic controls over convection in an inter-Andean valley in northern South America. *Mon. Wea. Rev.*, **151**, 145–162, doi: 10.1175/MWR-D-21-0231.1.

Gorja, M. M. K., V. S. Challa, Y. Viswanadhapalli, et al., 2023: Sensitivity of cloud microphysics on the simulation of heavy rainfall in WRF- a case study for the 7–10 August 2019 event over Kerala, India. *Atmos. Res.*, **288**, 106715, doi: 10.1016/j.atmosres.2023.106715.

Guo, Z. Y., J. Fang, X. G. Sun, et al., 2019: Sensitivity of summer precipitation simulation to microphysics parameterization over eastern China: Convection-permitting regional climate simulation. *J. Geophys. Res. Atmos.*, **124**, 9183–9204, doi: 10.1029/2019JD030295.

Gutowski, W. J., P. A. Ullrich, A. Hall, et al., 2020: The ongoing need for high-resolution regional climate models: Process understanding and stakeholder information. *Bull. Amer. Meteor. Soc.*, **101**, E664–E683, doi: 10.1175/BAMS-D-19-0113.1.

Halder, M., A. Hazra, P. Mukhopadhyay, et al., 2015: Effect of the

better representation of the cloud ice-nucleation in WRF microphysics schemes: A case study of a severe storm in India. *Atmos. Res.*, **154**, 155–174, doi: 10.1016/j.atmosres.2014.10.022.

Hernández-Deckers, D., 2022: Features of atmospheric deep convection in northwestern South America obtained from infrared satellite data. *Quart. J. Roy. Meteor. Soc.*, **148**, 338–350, doi: 10.1002/qj.4208.

Hong, S. Y., J. H. Lim, J. O. Lim, et al., 2006a: The WRF single-moment 6-class microphysics scheme (WSM6). *J. Korean Meteor. Soc*., **42**, 129–151.

Hong, S. Y., Y. Noh, and J. Dudhia, 2006b: A new vertical diffusion package with an explicit treatment of entrainment processes. *Mon. Wea. Rev.*, **134**, 2318–2341, doi: 10.1175/MWR3199.1.

Hoyos, C. D., L. I. Ceballos, J. S. Pérez-Carrasquilla, et al., 2019: Meteorological conditions leading to the 2015 Salgar flash flood: lessons for vulnerable regions in tropical complex terrain. *Nat. Hazards Earth Syst. Sci.*, **19**, 2635–2665, doi: 10.5194/nhess-19-2635-2019.

Hoyos, I., F. Dominguez, J. Cañón-Barriga, et al., 2018: Moisture origin and transport processes in Colombia, northern South America. *Climate Dyn.*, **50**, 971–990, doi: 10.1007/s00382-017-3653-6.

Hu, X.-M., Y. J. Huang, M. Xue, et al., 2023: Effects of lower troposphere vertical mixing on simulated clouds and precipitation over the Amazon during the wet season. *J. Geophys. Res. Atmos.*, **128**, e2023JD038553, doi: 10.1029/2023JD038553.

Huang, Y. J., Y. P. Wang, L. L. Xue, et al., 2020: Comparison of three microphysics parameterization schemes in the WRF model for an extreme rainfall event in the coastal metropolitan City of Guangzhou, China. *Atmos. Res.*, **240**, 104939, doi: 10.1016/j.atmosres.2020.104939.

Jaramillo, L., G. Poveda, and J. F. Mejía, 2017: Mesoscale convective systems and other precipitation features over the tropical Americas and surrounding seas as seen by TRMM. *Int. J. Climatol.*, **37**, 380–397, doi: 10.1002/joc.5009.

Jiménez, P. A., J. Dudhia, J. F. González-Rouco, et al., 2012: A revised scheme for the WRF surface layer formulation. *Mon. Wea. Rev.*, **140**, 898–918, doi: 10.1175/MWR-D-11-00056.1.

Jo, K.-R., K.-S. Pak, S.-N. Ri, et al., 2023: Impact of microphysics schemes on prediction of an extreme heavy rainfall event over the Democratic People's Republic of Korea: A case study using WRF model. *Meteor. Atmos. Phys.*, **135**, 36, doi: 10.1007/s00703-023-00961-6.

Junquas, C., M. B. Heredia, T. Condom, et al., 2022: Regional climate modeling of the diurnal cycle of precipitation and associated atmospheric circulation patterns over an Andean glacier region (Antisana, Ecuador). *Climate Dyn.*, **58**, 3075–3104, doi: 10.1007/s00382-021-06079-y.

Karki, R., S. U. Hasson, L. Gerlitz, et al., 2018: WRF-based simulation of an extreme precipitation event over the Central Himalayas: atmospheric mechanisms and their representation by microphysics parameterization schemes. *Atmos. Res.*, **214**, 21–35, doi: 10.1016/j.atmosres.2018.07.016.

Khain, A. P., K. D. Beheng, A. Heymsfield, et al., 2015: Representation of microphysical processes in cloud-resolving models: Spectral (bin) microphysics versus bulk parameterization. *Rev. Geophys.*, **53**, 247–322, doi: 10.1002/2014RG000468.

Klein, C., D. Heinzeller, J. Bliefernicht, et al., 2015: Variability of West African monsoon patterns generated by a WRF multi-physics ensemble. *Climate Dyn.*, **45**, 2733–2755, doi: 10.1007/s00382-015-2505-5.

L'Ecuyer, T. S., Y. Hang, A. V. Matus, et al., 2019: Reassessing the effect of cloud type on earth's energy balance in the age of active spaceborne observations. Part I: Top of atmosphere and surface. *J. Climate*, **32**, 6197–6217, doi: 10.1175/JCLI-D-18-0753.1.

Lehner, M., and M. W. Rotach, 2018: Current challenges in understanding and predicting transport and exchange in the atmosphere over mountainous terrain. *Atmosphere*, **9**, 276, doi: 10.3390/atmos9070276.

Liu, D. Q., B. Yang, Y. C. Zhang, et al., 2018: Combined impacts of convection and microphysics parameterizations on the simulations of precipitation and cloud properties over Asia. *Atmos. Res.*, **212**, 172–185, doi: 10.1016/j.atmosres.2018.05.017.

Liu, S., Yin, Y., Xiao, H., et al., 2021: The effects of ice nucleation on the microphysical processes and precipitation for a heavy rainfall event in Beijing. *Atmos. Res.*, **253**, 105476, doi: 10.1016/j.atmosres.2021.105476.

Liu, Y., X. Chen, Q. Li, et al., 2020: Impact of different microphysics and cumulus parameterizations in WRF for heavy rainfall simulations in the central segment of the Tianshan Mountains, China. *Atmos. Res.*, **244**, 105052, doi: 10.1016/j.atmosres.2020.105052.

Liu, Y., X. Chen, Q. Li, et al., 2020: Impact of different microphysics and cumulus parameterizations in WRF for heavy rainfall simulations in the central segment of the Tianshan Mountains, China. *Atmos. Res*., **244**, 105052, doi: 10.1016/j.atmosres.2020.105052.

Martínez, J. A., J. C. Camacho, D. Vasquez, et al., 2021: Simulation of mesoscale convective systems near the tropical Andes: Insights from convection-permitting simulations of two events. Available online at https://doi.org/10.5194/egusphere-egu21-10264. Accessed on 7 July 2024.

Martínez, J. A., P. A. Arias, C. Junquas, et al., 2022: The Orinoco low-level jet and the cross-equatorial moisture transport over tropical South America: Lessons from seasonal WRF simulations. *J. Geophys. Res. Atmos.*, **127**, e2021JD035603, doi: 10.1029/2021JD035603.

Martínez-Castro, D., S. Kumar, J. L. Flores Rojas, et al., 2019: The impact of microphysics parameterization in the simulation of two convective rainfall events over the Central Andes of Peru using WRF-ARW. *Atmosphere*, **10**, 442, doi: 10.3390/atmos10080442.

Mejía, J. F., and G. Poveda, 2020: Upper-air measurements at Nuquí, Colombia. Available online at https://doi.org/10.26023/M951-SXZK-NF0N. Accessed on 7 July 2024.

Mejía, J. F., J. Yepes, J. J. Henao, et al., 2021: Towards a mechanistic understanding of precipitation over the far eastern tropical Pacific and western Colombia, one of the rainiest spots on Earth. *J. Geophys. Res. Atmos.*, **126**, e2020JD033415, doi: 10.1029/2020JD033415.

Min, L. X., Q. L. Min, and Y. Y. Du, 2022: Evaluation of model summertime boundary layer cloud development over complex terrain in New York State. *Wea. Forecasting*, **37**, 2195–2207, doi: 10.1175/WAF-D-21-0172.1.

Mlawer, E. J., S. J. Taubman, P. D. Brown, et al., 1997: Radiative

transfer for inhomogeneous atmospheres: RRTM, a validated correlated-k model for the longwave. *J. Geophys. Res. Atmos.*, **102**, 16,663–16,682, doi: 10.1029/97JD00237.

Mohan, P. R., C. V. Srinivas, V. Yesubabu, et al., 2019: Tropical cyclone simulations over Bay of Bengal with ARW model: Sensitivity to cloud microphysics schemes. *Atmos. Res.*, **230**, 104651, doi: 10.1016/j.atmosres.2019.104651.

Morrison, H., G. Thompson, and V. Tatarskii, 2009: Impact of cloud microphysics on the development of trailing stratiform precipitation in a simulated squall line: Comparison of one- and two-moment schemes. *Mon. Wea. Rev.*, **137**, 991–1007, doi: 10.1175/2008MWR2556.1.

Morrison, H., M. Van Lier-Walqui, A. M. Fridlind, et al., 2020: Confronting the challenge of modeling cloud and precipitation microphysics. *J. Adv. Model. Earth Syst.*, **12**, e2019MS001689, doi: 10.1029/2019MS001689.

Moya-Álvarez, A. S., R. Estevan, S. Kumar, et al., 2020: Influence of PBL parameterization schemes in WRF_ARW model on short-range precipitation's forecasts in the complex orography of Peruvian Central Andes. *Atmos. Res.*, **233**, 104708, doi: 10.1016/j.atmosres.2019.104708.

Nakanishi, M., and H. Niino, 2006: An improved Mellor–Yamada level-3 model: Its numerical stability and application to a regional prediction of advection fog. *Bound.-Layer Meteor.*, **119**, 397–407, doi: 10.1007/s10546-005-9030-8.

NASA, 2017: NCEP/CPC L3 half hourly 4km global (60S–60N) merged IR V1 (GPM_MERGIR), doi: 10.5067/P4HZB9N27EKU.

NASA, 2019: GPM Imerg Final Precipitation L3 1 day 0.1 degree x 0.1 degree v06, doi: 10.5067/GPM/IMERGDF/DAY/06.

Niu, G.-Y., Z.-L. Yang, K. E. Mitchell, et al., 2011: The community Noah land surface model with multiparameterization options (Noah-MP): 1. Model description and evaluation with local-scale measurements. *J. Geophys. Res. Atmos.*, **116**, D12109, doi: 10.1029/2010JD015139.

Olson, J. B., J. S. Kenyon, W. A. Angevine, et al., 2019: A Description of the MYNN-EDMF Scheme and the Coupling to Other Components in WRF–ARW. NOAA Technical Memorandum OAR GSD-61, NOAA, Bouder, 1–21.

Oreopoulos, L., N. Cho, and D. Lee, 2017: New insights about cloud vertical structure from CloudSat and CALIPSO observations. *J. Geophys. Res. Atmos.*, **122**, 9280–9300, doi: 10.1002/2017JD026629.

Park, J., D.-H. Cha, M. K. Lee, et al., 2020: Impact of cloud microphysics schemes on tropical cyclone forecast over the western North Pacific. *J. Geophys. Res. Atmos.*, **125**, e2019JD032288, doi: 10.1029/2019JD032288.

Podeti, S. R., S. S. V. S. Ramakrishna, Y. Viswanadhapalli, et al., 2020: Sensitivity of cloud microphysics on the simulation of a monsoon depression over the Bay of Bengal. *Pure Appl. Geophys.*, **177**, 5487–5505, doi: 10.1007/s00024-020-02557-2.

Poveda, G., P. R. Waylen, and R. S. Pulwarty, 2006: Annual and inter-annual variability of the present climate in northern South America and southern Mesoamerica. *Palaeogeogr. Palaeoclimatol. Palaeoecol.*, **234**, 3–27, doi: 10.1016/j.palaeo.2005.10.031.

Poveda, G., L. Jaramillo, and L. F. Vallejo, 2014: Seasonal precipitation patterns along pathways of South American low-level jets and aerial rivers. *Water Resour. Res.*, **50**, 98–118, doi: 10.1002/2013WR014087.

Prein, A. F., M. Ge, A. R. Valle, et al., 2022: Towards a unified setup to simulate mid-latitude and tropical mesoscale convective systems at kilometer-scales. *Earth Space Sci.*, **9**, e2022EA002295, doi: 10.1029/2022EA002295.

Qian, Y., H. P. Yan, L. K. Berg, et al., 2016: Assessing impacts of PBL and surface layer schemes in simulating the surface–atmosphere interactions and precipitation over the tropical ocean using observations from AMIE/DYNAMO. *J. Climate*, **29**, 8191–8210, doi: 10.1175/JCLI-D-16-0040.1.

Que, L. J., W. L. Que, and J. M. Feng, 2016: Intercomparison of different physics schemes in the WRF model over the Asian summer monsoon region. *Atmos. Oceanic Sci. Lett.*, **9**, 169–177, doi: 10.1080/16742834.2016.1158618.

Reshmi Mohan, P., C. V. Srinivas, V. Yesubabu, et al., 2018: Simulation of a heavy rainfall event over Chennai in Southeast India using WRF: Sensitivity to microphysics parameterization. *Atmos. Res.*, **210**, 83–99, doi: 10.1016/j.atmosres.2018.04.005.

Riley Dellaripa, E. M., E. D. Maloney, and C. A. DeMott, 2023: The diurnal cycle of east Pacific convection, moisture, and CYGNSS wind speed and fluxes. *J. Geophys. Res. Atmos.*, **128**, e2022JD038133, doi: 10.1029/2022JD038133.

Roberts, N. M., and H. W. Lean, 2008: Scale-selective verification of rainfall accumulations from high-resolution forecasts of convective events. *Mon. Wea. Rev.*, **136**, 78–97, doi: 10.1175/2007MWR2123.1.

Ruiz-Vásquez, M., P. A. Arias, J. A. Martínez, et al., 2020: Effects of Amazon basin deforestation on regional atmospheric circulation and water vapor transport towards tropical South America. *Climate Dyn.*, **54**, 4169–4189, doi: 10.1007/s00382-020-05223-4.

Rydbeck, A. V., E. D. Maloney, and G. J. Alaka, 2017: In situ Initiation of east Pacific easterly waves in a regional model. *J. Atmos. Sci.*, **74**, 333–351, doi: 10.1175/JAS-D-16-0124.1.

Sakamoto, M. S., T. Ambrizzi, and G. Poveda, 2011: Moisture sources and life cycle of convective systems over western Colombia. *Adv. Meteor.*, **2011**, 890759, doi: 10.1155/2011/890759.

Shu, W. X., D. H. Fu, H. Xiao, et al., 2023: Cloud microphysical processes and atmospheric water budget during the 20 July 2021 extreme precipitation event in Zhengzhou, China. *J. Meteor. Res.*, **37**, 722–742, doi: 10.1007/s13351-023-2166-y.

Skamarock, W. C., J. B. Klemp, J. Dudhia, et al., 2019: A Description of the Advanced Research WRF Model Version 4. NCAR Technical Notes NCAR/TN-556+STR, NCAR, Boulder, 1–5.

Srinivas, C. V., V. Yesubabu, D. Hari Prasad, et al., 2018: Simulation of an extreme heavy rainfall event over Chennai, India using WRF: Sensitivity to grid resolution and boundary layer physics. *Atmos. Res.*, **210**, 66–82, doi: 10.1016/j.atmosres.2018.04.014.

Stensrud, D. J., 2007: *Parameterization Schemes: Keys to Understanding Numerical Weather Prediction Models*. Cambridge University Press, Cambridge, 138–304, doi: 10.1017/CBO9780511812590.

Stull, R. B., 1988: *An Introduction to Boundary Layer Meteorology*. Springer, Dordrecht, 200 pp.

Taraphdar, S., and O. M. Pauluis, 2021: Impact of planetary

boundary layer and cloud microphysics on the sensitivity of monsoon precipitation using a gray-zone regional model. *Earth Space Sci.*, **8**, e2020EA001535, doi: 10.1029/2020EA001535.

Thomas, B., Y. Viswanadhapalli, C. V. Srinivas, et al., 2021: Cloud resolving simulation of extremely heavy rainfall event over Kerala in August 2018–Sensitivity to microphysics and aerosol feedback. *Atmos. Res.*, **258**, 105613, doi: 10.1016/j.atmosres.2021.105613.

Thompson, G., P. R. Field, R. M. Rasmussen, et al., 2008: Explicit forecasts of winter precipitation using an improved bulk microphysics scheme. Part II: Implementation of a new snow parameterization. *Mon. Wea. Rev.*, **136**, 5095–5115, doi: 10.1175/2008MWR2387.1.

Tian, J. Y., J. Liu, J. H. Wang, et al., 2017: A spatio-temporal evaluation of the WRF physical parameterisations for numerical rainfall simulation in semi-humid and semi-arid catchments of Northern China. *Atmos. Res.*, **191**, 141–155, doi: 10.1016/j.atmosres.2017.03.012.

Torrealba Rincón, E. R., and J. A. Amador Astúa, 2010: La corriente en chorro de bajo nivel sobre los Llanos Venezolanos de Sur América. *Revista Climatol.*, **10**, 1–20. (in Spanish)

Urrea, V., A. Ochoa, and O. Mesa, 2019: Seasonality of rainfall in Colombia. *Water Resour. Res.*, **55**, 4149–4162, doi: 10.1029/2018WR023316.

Valencia, S., D. E. Marín, D. Gómez, et al., 2023: Spatio-temporal assessment of gridded precipitation products across topographic and climatic gradients in Colombia. *Atmos. Res*, **285**, 106643, doi: 10.1016/j.atmosres.2023.106643.

Vallejo-Bernal, S. M., V. Urrea, J. M. Bedoya-Soto, et al., 2021: Ground validation of TRMM 3B43 V7 precipitation estimates over Colombia. Part I: Monthly and seasonal timescales. *Int. J. Climatol.*, **41**, 601–624, doi: 10.1002/joc.6640.

Wang, R., Y. T. Zhu, F. X. Qiao, et al., 2021: High-resolution simulation of an extreme heavy rainfall event in Shanghai using the weather research and forecasting model: Sensitivity to planetary boundary layer parameterization. *Adv. Atmos. Sci.*, **38**, 98–115, doi: 10.1007/s00376-020-9255-y.

Wilks, D. S., 2011. *Statistical Methods in the Atmospheric Sciences*. 3rd Ed., Elsevier, Amsterdam, 306–311.

Woodhams, B. J., C. E. Birch, J. H. Marsham, et al., 2018: What is the added value of a convection-permitting model for forecasting extreme rainfall over tropical east Africa. *Mon. Wea. Rev.*, **146**, 2757–2780, doi: 10.1175/MWR-D-17-0396.1.

Yáñez-Morroni, G., J. Gironás, M. Caneo, et al., 2018: Using the weather research and forecasting (WRF) model for precipitation forecasting in an Andean region with complex topography. *Atmosphere*, **9**, 304, doi: 10.3390/atmos9080304.

Yang, B., L. K. Berg, Y. Qian, et al., 2019: Parametric and structural sensitivities of turbine-height wind speeds in the boundary layer parameterizations in the weather research and forecasting model. *J. Geophys. Res. Atmos.*, **124**, 5951–5969, doi: 10.1029/2018JD029691.

Yang, Q., R. A. Jr. Houze, L. R. Leung, et al., 2017: Environments of long-lived mesoscale convective systems over the Central United States in convection permitting climate simulations. *J. Geophys. Res. Atmos.*, **122**, 13,288–13,307, doi: 10.1002/2017JD027033.

Yepes, J., G. Poveda, J. F. Mejía, et al., 2019: CHOCO-JEX: A research experiment focused on the Chocó low-level jet over the far eastern Pacific and western Colombia. *Bull. Amer. Meteor. Soc.*, **100**, 779–796, doi: 10.1175/BAMS-D-18-0045.1.

Yepes, J., J. F. Mejía, B. Mapes, et al., 2020: Gravity waves and other mechanisms modulating the diurnal precipitation over one of the rainiest spots on Earth: Observations and simulations in 2016. *Mon. Wea. Rev.*, **148**, 3933–3950, doi: 10.1175/MWR-D-19-0405.1.

Zhang, C. X., and Y. Q. Wang, 2017: Projected future changes of tropical cyclone activity over the western North and South Pacific in a 20-km-mesh regional climate model. *J. Climate*, **30**, 5923–5941, doi: 10.1175/JCLI-D-16-0597.1.

Zhao, D. J., Y. B. Yu, J. F. Yin, et al., 2020: Effects of microphysical latent heating on the rapid intensification of Typhoon Hato (2017). *J. Meteor. Res.*, **34**, 368–386, doi: 10.1007/s13351-020-9076-z.

Zhu, Y. T., F. X. Qiao, Y. J. Liu, et al., 2022: The impacts of multi-physics parameterization on forecasting heavy rainfall induced by weak landfalling Typhoon Rumbia (2018). *Atmos. Res.*, **265**, 105883, doi: 10.1016/j.atmosres.2021.105883.

Tech & Copy Editor: Zhirong CHEN